Geochemical, microthermometric, and isotopic constraints on the origin of fluorite deposits in central Anatolia, Turkey

Pelin COŞANAY[1], Ece KIRAT[1], Nihal ÇEVİK[2], Ceyda KIZILKANAT[1], Halim MUTLU[1,]*, Şükrü KOÇ[1]

[1]Department of Geological Engineering, Faculty of Engineering, Ankara University, Gölbaşı, Ankara, Turkey
[2]General Directorate of Mineral Research and Exploration, Ankara, Turkey

Abstract: We investigate rare earth element geochemistry, microthermometric characteristics, and radiogenic isotope systematics of fluorites and stable isotope compositions of gangue minerals from several fluorite deposits in central Turkey. In the deposits, fluorite is the main ore mineral and it is accompanied by quartz, calcite, and minor pyrite and barite. Veins are represented by three different fluorite types based on their color. Total REY contents of fluorites are highly variable, ranging from 24 to 693 ppm. LREE concentrations of fluorites of all colors are similar but medium and heavy REE abundances of green fluorites are nearly an order of magnitude greater than in both host rocks and purple and yellow fluorites, indicating multiple sources for crystallization. REEs show significant fractionation and purple fluorites with relatively low HREE contents were likely precipitated at an earlier stage. As crystallization continued, green fluorites were nucleated because of ion exchange of LREEs with the host rock/minerals. Fluid inclusions yielded a wide range of homogenization temperatures from 86 °C to 292 °C and salinities from 0 to 20 wt.% NaCl equiv. The $^{87}Sr/^{86}Sr$ ratios of fluorites, varying from 0.707627 to 0.709380, overlap with the range of host rocks. $^{143}Nd/^{144}Nd$ values suggest two populations: purple fluorites with less radiogenic and green fluorites with more radiogenic Nd isotope ratios. The Sr-Nd isotope systematics of Bayındır fluorites are consistent with that of the Bayındır syenite, indicating that hydrothermal solutions progressively reacted with the host rock until equilibrium was established. $\delta^{18}O$ values of quartz are slightly higher than the magmatic range. $\delta^{13}C$ and $\delta^{18}O$ of calcites fall into the range of marine carbonates. $\delta^{34}S$ values of barites indicate derivation from diverse reservoirs changing from marine to terrestrial sources. In contrast, sulfur in pyrites points to a magmatic origin. Therefore, is it suggested that magmatic fluids to some extent contributed to the precipitation of fluorite veins.

Key words: Fluorite, central Anatolia, geochemistry, radiogenic-stable isotope, fluid inclusions

1. Introduction

Fluorite occurs in various ore deposits with different host rock lithologies and modes of deposition. The type of deposits varies from open-space filling (e.g., veins, fissures) hydrothermal mineralizations formed by low-temperature, moderate- to high-salinity fluids to pegmatite-pneumatolytic vein mineralizations deposited under high-temperature conditions (Hill et al., 2000). Fluorite is a common accessory or gangue mineral although it may also form as a major ore mineral.

Fluorite is a very informative mineral since it allows determining not only the temperature but also the timing of mineralization. The Sm-Nd isochron technique is successfully applied to fluorite and accompanying calcite for dating episodes of mineralization (Chesley et al., 1994; Munoz et al., 2005). However, Barker et al. (2009) suggested that, because of incomplete equilibration or mixing, Nd isotope systematics may be diversified, failing to determine ages using Sm-Nd isochrons.

The majority of fluorite deposits in Turkey are hosted by subduction-related alkaline magmatic rocks, which were formed by melting of subducting oceanic slab along the Neotethyan suture zone (Kadıoğlu et al., 2006). Melting of the oceanic crust at depths below about 300 km is proposed to have generated K-rich igneous rock, which in turn gave rise to increasing alkalinity of subduction-related plutonic rocks. As a result of metasomatism involving hydrous oceanic crust, some of the metamorphosed mantle minerals were altered to phlogopite, which contains nearly 3% fluorine (e.g., Edgar and Arima, 1985). Fluorine originating from the melting of phlogopite at great depths of subduction regions is moved upward by hydrothermal fluids to precipitate in fluorite under favorable geologic conditions.

Fluorite vein deposits in central Turkey occur in the Central Anatolian Crystalline Complex (Figure 1), which hosts several calc-alkaline and alkaline intrusive bodies. Geochemical and microthermometric characteristics of
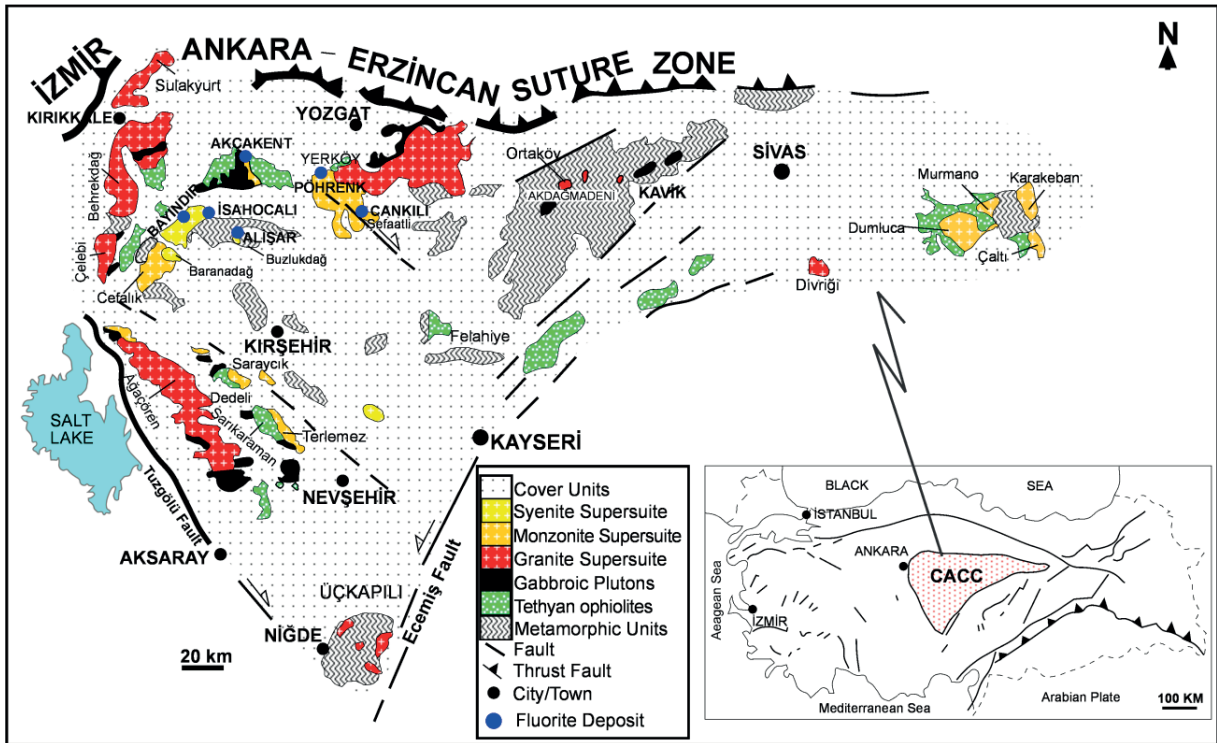
Figure 1. Map showing the geology (from Kadıoğlu et al., 2006) and locations of studied fluorite deposits in central Anatolia. CACC: Central Anatolian Crystalline Complex.

fluorite deposits have been the subject of numerous studies over the last three decades (e.g., Yaman, 1985; Genç, 2006; Koç et al., 2007; Şaşmaz and Yavuz, 2007; Uras, 2007). These works have propounded that central Anatolian fluorites precipitated from low- to moderate-temperature fluids (80 to 360 °C) with a wide range of salinity (1 to 24 wt.% NaCl equiv.) and the rare earth element distributions of fluorites commonly indicate a hydrothermal type for the mineralizing fluids. Despite intensive research on mineralogical and geochemical characteristics of these mineralizations, there are limited data on the source of fluids that are responsible for fluorite deposition.

Since isotopes of elements with large atomic numbers such as Sr are not significantly fractionated during ore deposition, they are very helpful for determining the isotopic composition of host rocks with which they are equilibrated or interacting. Consequently, the use of radiogenic isotopes for genetic investigation of hydrothermal deposits takes priority over trace element concentrations, which are relatively more affected by magmatic processes such as fractional crystallization. Taking this into account, central Anatolian fluorites with a great variety of colors were examined with a particular emphasis on their REY abundances and Sr-Nd isotope

systematics. Results of these analyses were combined with data on homogenization temperatures of fluorites and stable isotope compositions of secondary minerals (e.g., sulfate, sulfide, and quartz) in order to assess the evolution of the hydrothermal solutions that prevailed in the studied deposits.

2. Geologic setting

Tectonomagmatic evolution of Anatolia has been defined by the closure of the Neotethyan Ocean, which gave rise to the Africa-Eurasia collision in the late Mesozoic and the Arabia-Anatolia collision in the Miocene (Şengör and Yılmaz, 1981). As a result, widespread coeval and postcollisional plutonism developed throughout Turkey.

Metamorphic rocks, ophiolites, and magmatic intrusions in central Anatolia are collectively called the Central Anatolian Crystalline Complex (CACC; Figure 1) (Göncüoğlu et al., 1991). The CACC is confined by the Tuzgölü fault to the west, the Ecemiş fault to the east, and the İzmir-Ankara-Erzincan suture to the north. The complex also includes several metamorphic massifs (e.g., Kırşehir, Akdağ, and Niğde massifs) and disjoined ophiolites of the Neotethyan convergence and it is surrounded on the peripheries by a number of curvilinear sedimentary basins

(e.g., Tuzgölü, Ulukışla, Çiçekdağı, and Sivas basins) that have been filled with marine and terrestrial sediments of various age (Görür et al., 1998).

According to Aydın et al. (1998) and Kadıoğlu et al. (2006), the composition of Late Cretaceous magmatism in the CACC changed from calc-alkaline to alkaline and the relative input of mafic magma in the origin of the magmatic rocks of the complex increased with time. They also suggested that magmatism shows temporal variations in composition varying from granite to syenite; the latter is further subdivided into silica-oversaturated/saturated to silica-undersaturated suites. Kadıoğlu et al. (2006) grouped the Late Cretaceous magmatic rocks in the CACC into granite, monzonite, and syenite supersuites. The granitic rocks comprising larger plutonic bodies are generally found in western and northern sections of the complex, whereas monzonite and syenite plutons are exposed in the middle part (Figure 1).

There are two contrasting suggestions for the geodynamic setting of CACC magmatic rocks. According to Boztuğ (1998), Yalınız et al. (1999), Köksal et al. (2001, 2004), Boztuğ et al. (2003, 2007), and İlbeyli et al. (2004), central Anatolian granitoids formed in a syn- to postcollisional geodynamic setting associated with the closure of the İzmir-Ankara-Erzincan ocean. On the other hand, Kadıoğlu et al. (2006) proposed that Late Cretaceous plutonic rocks in central Anatolia were emplaced following the obduction of Tethyan ophiolites and therefore their evolution preceded the continental collision in the

region. The dating of magmatism in central Anatolia was practiced in several studies. The resulting ages vary in a wide range from 58.7 Ma (Cankılı monzonite; Boztuğ and Harlavan, 2008) to 84.1 Ma (Ağaçören granite; Köksal et al., 2012). The geochemical and geochronological data from the plutonic rocks in the CACC indicate both syn- and postcollisional magmatism. The central Anatolian plutons host several ore deposits, which comprise skarn and various polymetallic mineralizations (e.g., Pb-Zn, Fe, and Fe-W skarns) (Erler and Bayhan, 1998; Kuşçu and Erler, 1998), some of which are associated with vein fluorite deposits (Genç, 2006; Koç et al., 2007; Şaşmaz and Yavuz, 2007).

3. Sampling and analytical methods
All fluorite and host rock samples were collected from exposed veins (Figures 2a–2d), except for the Cankılı and Akçakent deposits, where samples were taken from mine shafts.

Fluid inclusion analysis was performed using a Linkam THMSG-600 model liquid nitrogen freezing-heating stage installed on a Leica DM 2500M polarizing microscope at the fluid inclusion laboratory of the Geology Department of Ankara University. The temperature range of the stage is from –196 °C to 600 °C. The stage was calibrated with pure synthetic H_2O and H_2O-NaCl synthetic fluid inclusion standards at temperatures of –56.6 °C, –21.2 °C, –10.7 °C, 0.0 °C, and 374.1 °C. The accuracy of the homogenization temperature (Th_{H2O}) is 4.0 °C, the H_2O
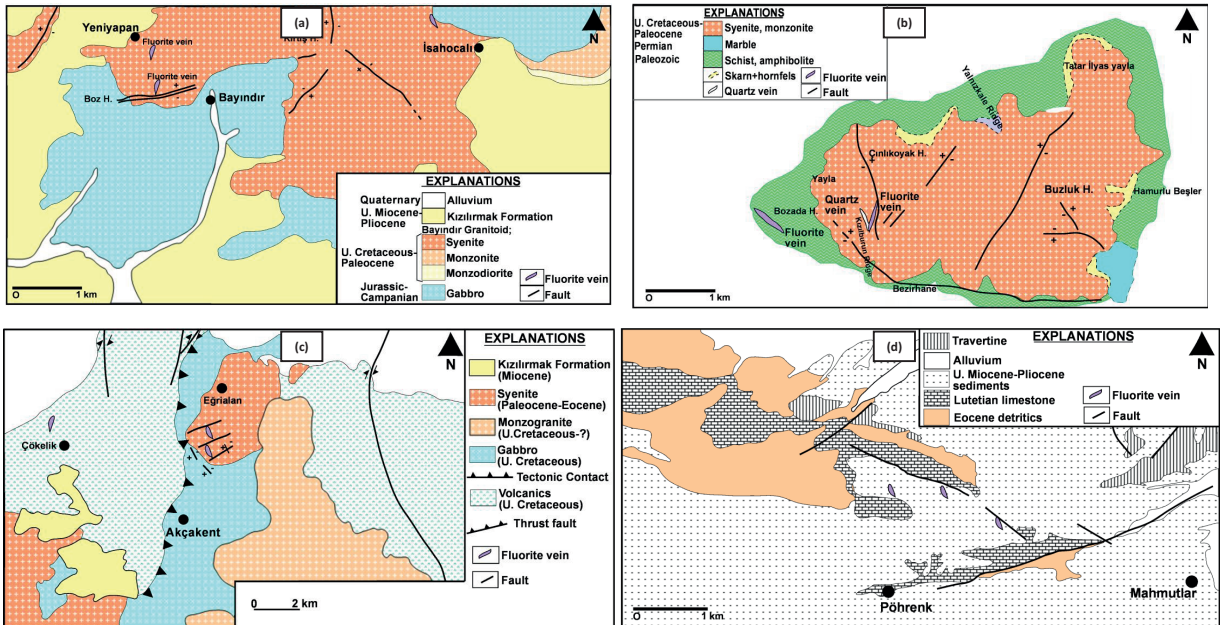
Figure 2. Geology maps of studied fluorite deposits: a) Bayındır, Yeniyapan, and İsahocalı deposits (from Koç et al., 2007); b) Alişar deposit (from Özgenç et al., 2009); c) Akçakent deposit (from Yılmaz and Boztuğ, 1998); and d) Pöhrenk deposit (from Genç, 2006).

3

final melting ice temperature (Tm$_{H2O}$) is ±0.1 °C, and the H$_2$O-NaCl eutectic temperature (Te) is ±0.8 °C. Fluid inclusion assemblages were described using the criteria of Roedder (1984). Inclusion types were petrographically determined prior to measurements. A total of 19 doubly polished wafers prepared from fluorite were used for the determinations. During the measurements, a vast majority of the inclusions homogenized into liquid phase and no boiling was recognized. Since fluorite veins were formed as open space-filling and the emplacement depth of mineralizing fluids is uncertain, presumably a minimum overburden would be sufficient to prevent boiling during the vein formation. Therefore, homogenization temperatures are assumed to be close to the trapping temperatures, necessitating little or no pressure correction (e.g., Hein et al., 1990).

Trace element analysis of samples was carried out at ACME Analytical Laboratories, Canada, by ICP-MS method with detection limit ranging from 0.01 to 0.05 ppm. Samples (0.25 g split) were heated in nitric, hydrochloric, and hydrofluoric acids to fuming and taken to dryness. The residue was dissolved in HCl.

^{87}Sr/^{86}Sr compositions of fluorites and magmatic rocks were analyzed at the central laboratories of Middle East Technical University using the protocols and procedures described by Köksal and Göncüoğlu (2008). Strontium was separated in Teflon columns in 2.5 N HCl with 2 mL of Bio-Rad AG50 W-X12, 100–200 mesh resin. The REE fraction was collected from Sr cation exchange columns with 6 N HCl after Sr was separated. Strontium was loaded on single Re-filaments with a Ta-activator and 0.005 N H$_3$PO$_4$ and measured in static mode. Sr ratios were normalized to ^{86}Sr/^{88}Sr = 0.1194. Sr isotope ratios were measured using a Thermo-Fisher Triton thermal ionization mass spectrometer, and standard errors were presented at 2-sigma level. During the analysis Sr NBS 987 standard was measured as 0.710251 ± 8 (n = 3).

δ^{18}O (relative to VSMOW), δ^{13}C – δ^{18}O (relative to VPDB), and δ^{34}S (relative to VCDT) analyses of quartz, calcite, and barite-pyrite were measured at the GNS Science Laboratory, New Zealand. A laser fluorination line was used for silicates (with analytical precision of 0.1‰) and the GVI Isoprime mass spectrometer coupled with AquaPrep was used for carbonates (with precisions of 0.3‰ and 0.1‰ for δ^{13}C and δ^{18}O) and sulfur phases (with analytical precision of 0.3‰).

4. Geologic and mineralogical characteristic of fluorite deposits

Fluorite samples were collected from the Bayındır, Yeniyapan, İsahocalı, Alişar, Pöhrenk, and Akçakent deposits in the Kırşehir district and the Cankılı deposit in the Yozgat district (Figure 1; Table 1). Except for the Bayındır, Yeniyapan, İsahocalı, and Alişar deposits, fluorite ores in all other mineralizations are currently being exploited. The studied deposits are hosted in alkaline magmatic rocks such as syenite and monzonite with the exception of the Pöhrenk deposit, where fluorite occurs within limestone.

Metamorphites of the Kırşehir Massif consisting of schist, marble, quartzite, and metachert form the basement in the Kaman area (Kırşehir district) (Seymen, 1981). They are intruded by the Bayındır syenite pluton (69.8 Ma; Kadıoğlu et al., 2006), which is composed of orthoclase, plagioclase, amphibole, melanite, clinopyroxene, nepheline, and/or cancrinite. Fluorite mineralizations within this pluton formed in three different deposits: the Yeniyapan, Bayındır, and İsahocalı deposits extending from west to east (Figure 2a). The Bayındır and Yeniyapan deposits, located ~250 m apart from each other, occur as two separate bodies along an E-W-trending normal fault cutting the Bayındır syenite. Fluorite ore was produced previously from a gallery and from a disused shaft (Figure 3a). The total length of deposits is approximately 500 m. Fluorite ores are exclusively of the vein-filling type, occurring within NW- and NE-extending, steeply dipping fracture sets (Figure 3b).

Fluorite crystals occur in different colors; dark purple (violet) and green fluorites are the main varieties (Figure 3c). In mineralized veins fluorite is commonly accompanied by quartz. In addition to monomineralic veins, fluorite crystals also form concentric growth banding. Purple fluorites always occur as single veins, whereas green fluorites are rhythmically banded with purple fluorites, evidently reflecting changes in vein-fluid composition with time (Figure 3d). Mineralizations are usually irregular along any given vein and pinch out in short distances. Fluorite veins in the Bayındır area have surface extents ranging from 5 to about 25 m and thicknesses varying from a few centimeters to 20 cm (Figure 3c). No significant cross-cutting relation was recognized for the veins.

The İsahocalı deposit is located nearly 4 km east of the Bayındır-Yeniyapan deposits (Figures 1 and 2a). Fluorite veins within the Bayındır syenite are observed in several small-scale pits previously operated. In this deposit, veins vary in width from 1 to 2 cm. Although rare, lenticular fluorite veins with thicknesses of about 50 cm also occur (Figure 3e). In such veins, massive precipitates of purple fluorites are banded and intensely silicified and are locally separated by slivers of host rock. In some veins fluorite and quartz are precipitated in a crystal mesh, implying a cogenetic relationship between these two minerals (Figure 3f).

Zoned purple fluorites and fluorite crystal packets are entirely surrounded by massive quartz crystals (Figure 4a)

Table 1. Locations of studied fluorite deposits with fluorite type and host-rock data.

Deposit name	Sample no.	Sample type	Latitude (N)	Longitude (E)
Bayındır deposit	BYD1-1/1	Purple fluorite	33°49′55″	39°24′29″
	BYD1-1/21	Purple fluorite	33°49′55″	39°24′29″
	BYD1-1/22	Green fluorite	33°49′55″	39°24′29″
	BYD2-1/1	Purple fluorite	33°49′55″	39°24′29″
	BYD2-1/2	Green fluorite	33°49′55″	39°24′29″
	BYD3-1	Purple fluorite	33°49′58″	39°24′29″
	BYD3-2	Green fluorite	33°49′58″	39°24′29″
	BYD-3/1	Purple fluorite	33°49′58″	39°24′29″
	BYD-4/1	Purple fluorite	33°50′10″	39°24′29″
	BYD-4/2	Purple fluorite	33°50′10″	39°24′29″
	BYD-5/1	Purple fluorite	33°50′09″	39°24′31″
	BYD-5/2	Green fluorite	33°50′09″	39°24′31″
	BYD-6	Purple fluorite	33°50′21″	39°24′30″
	BYD-10	Syenite	33°52′08″	39°24′41″
İsahocalı	ISA-3	Purple fluorite	33°53′07″	39°25′26″
Alişar deposit	ALI-3/2	Purple fluorite	34°06′15″	39°25′16″
	ALI-4	Purple fluorite	34°06′03″	39°25′15″
	ALI-3/1-	Calcite	34°06′59″	39°24′19″
	ALI-10	Nepheline syenite	34°06′15″	39°25′16″
Akçakent deposit	AKC-1/1	Purple fluorite	34°06′29″	39°39′31″
	AKC-1/2	Green fluorite	34°06′29″	39°39′31″
	AKC-1/3	Green fluorite	34°06′06″	39°39′36″
	AKC-2/1	Green fluorite	34°06′34″	39°39′55″
	AKC-2/2	Green fluorite	34°06′34″	39°39′55″
	AKC-6	Green fluorite	34°01′32″	39°39′03″
	AKC-10	Syenite	34°06′39″	39°39′29″
Cankılı deposit	CAN-1	Green fluorite	34°41′09″	39°33′09″
	CAN-10	Monzonite	34°40′47″	39°33′00″
Pöhrenk deposit	PHR-1/1	Yellow fluorite	34°27′16″	39°26′44″
	PHR-2/1	Yellow fluorite	34°28′23″	39°26′17″
	PHR-2/2	Yellow fluorite	34°28′23″	39°26′17″
	PHR-10/2	Limestone	34°°28′23″	39°26′17″

or in some cases crystals with well-formed cleavage planes are cut by silica veins (Figure 4b). Because of pervasive hydrothermal alteration, most probably during the fluorite deposition, nepheline in syenite has been replaced by muscovite (Figures 4c and 4d). Silicification, kaolinization, and hematitization are the major alterations recognized along the crack zones.

The Alişar deposit is located on Buzlukdağ Hill, 20 km east of the Kaman area (Figures 1 and 2b). Fluorite veins occur within the Buzlukdağ intrusion (60.2 Ma; Boztuğ and Jonckheere, 2007), which is a silica-undersaturated alkaline syenite (Figure 5a) with mineralogical composition similar to that of the Bayındır pluton (Deniz and Kadıoğlu, 2016). The syenite intruded Paleozoic metamorphic rocks composed mainly of schist, gneiss, and marble. The normal faults that cut the intrusives are predominantly NE-SW and subordinately NW-SE trending. The pluton is also frequently cut by felsic and mafic dykes that extend
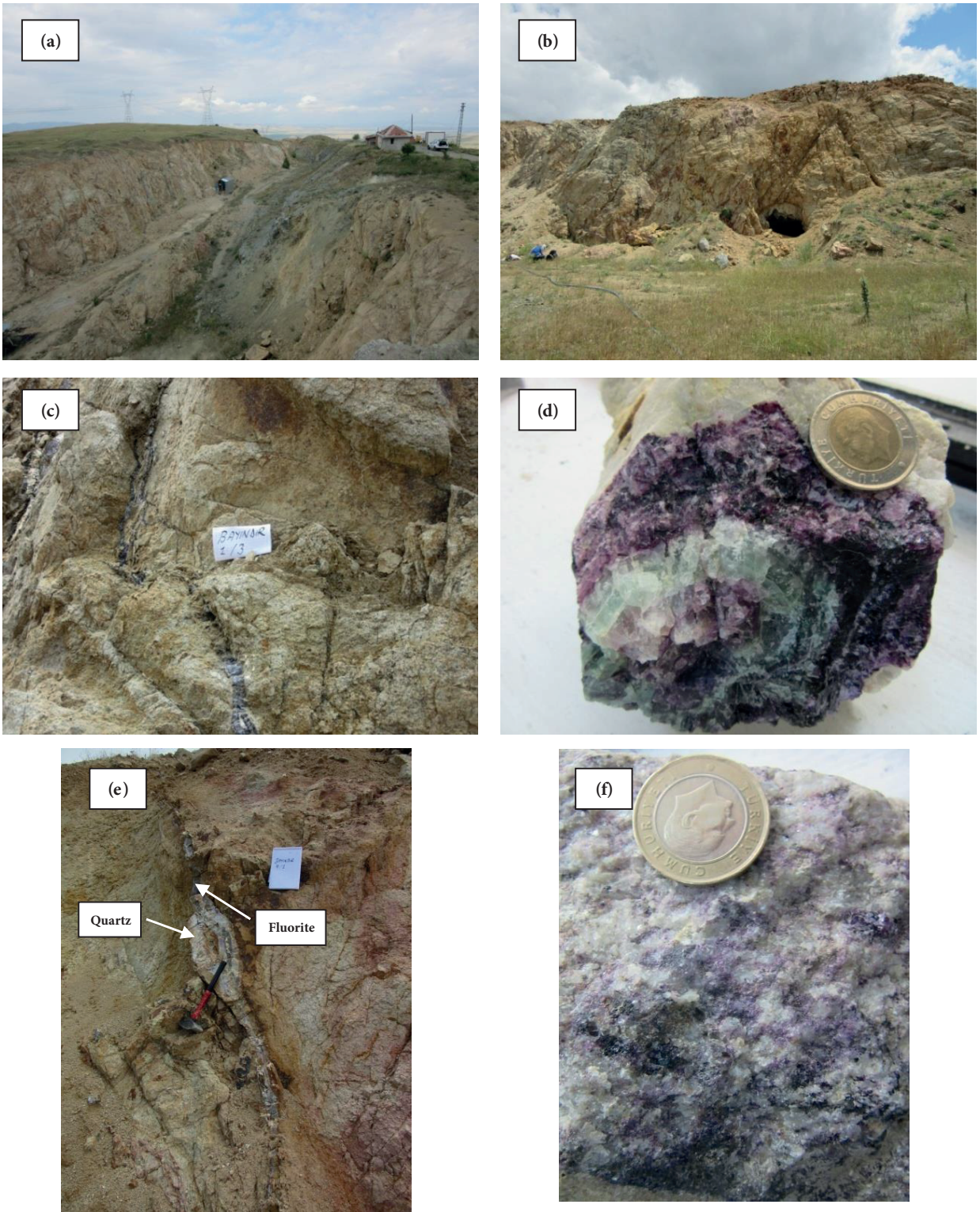
Figure 3. a) E-W striking normal fault in the Bayındır syenite; note the mine shaft at the center (looking from east). b) Main gallery excavated in syenite; fluorite veins within NW- and NE-extending fracture sets (looking from north). c) View of dark purple fluorite vein in the Bayındır syenite. d) Rhythmic banding of purple and green fluorites. e) Steeply dipping lenticular fluorite veins in the Yeniyapan deposit. f) Hand specimen showing cogenetic precipitation of fluorite and quartz in a crystal mesh (İsahocalı deposit).
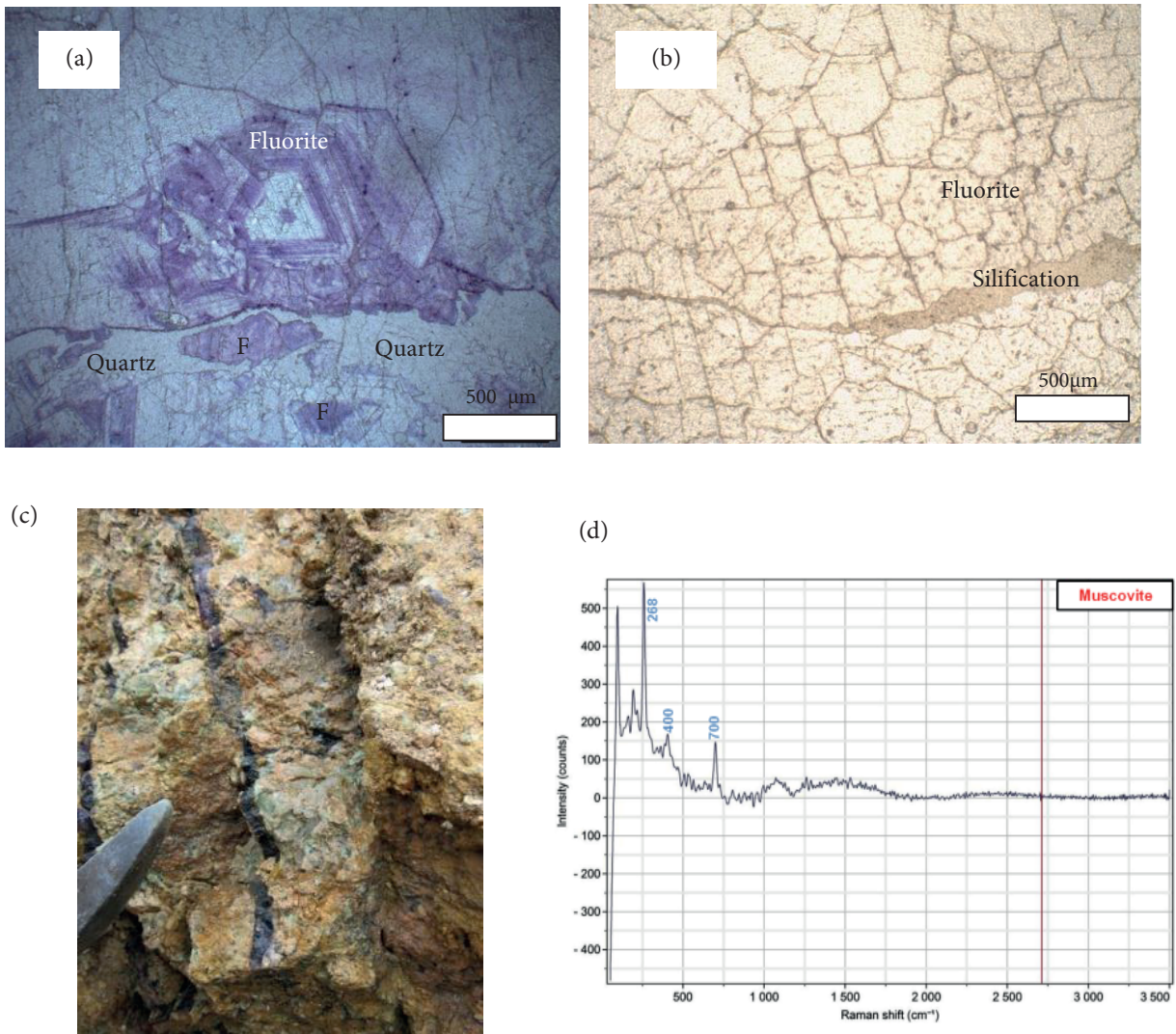
Figure 4. Photomicrographs for the textural properties of fluorite: a) zoned fluorite surrounded by interlocking quartz crystals (F: fluorite) and b) fluorite with prominent cleavage plane cut by silica veinlets, c) pervasive alteration in Bayındır syenite changing nepheline to muscovite (light green), d) Raman spectrum of muscovite mineral shown in (c).

nearly parallel to the faults. Several skarn facies (e.g., pyroxene-scapolite skarn, garnet-scapolite-pyroxene skarn, garnet-vesuvianite skarn) occur from the marble contact toward the syenite (Özgenç et al., 2009). Fluorite veins are recognized at the western part of the intrusive. Purple fluorites form drusy veins or coatings on the walls of fractures (Figure 5b), which are intensely kaolinized and hematitized. Veins are irregular and have widths of 1–2 cm. Quartz and rare calcite are the main gangue minerals (Figure 5c), accompanied by minor vein pyrite (Figure 5d).

The Akçakent deposit is located in the Çiçekdağı igneous complex (Figures 1 and 2c), which is composed of ophiolites, calc-alkaline series, alkaline series, and late alkaline dykes (Deniz et al., 2015; Deniz, 2016). The

igneous rocks of felsic and mafic compositions intruded the ophiolites. The calc-alkaline series are generally composed of monzonite and monzodiorite, whereas the alkaline series consists of syenites and feldspathoid-bearing gabbros. Basalts represent the late alkaline series. U-Pb dating of zircons yielded crystallization ages of 73 to 78 and 74 Ma for calc-alkaline and alkaline series, respectively, indicating that they are in coexistence and may have contemporarily originated from the same sources. The age of basalts from late alkaline series is dated at 63 Ma by the Ar-Ar method (Deniz et al., 2015). The fluorite deposits occur along several NW-SE extending normal faults at the contact between syenite and gabbro around the Eğrialan site, 2 km north of the town of Akçakent (Figure 2c). Although Akçakent fluorite veins have been well reported
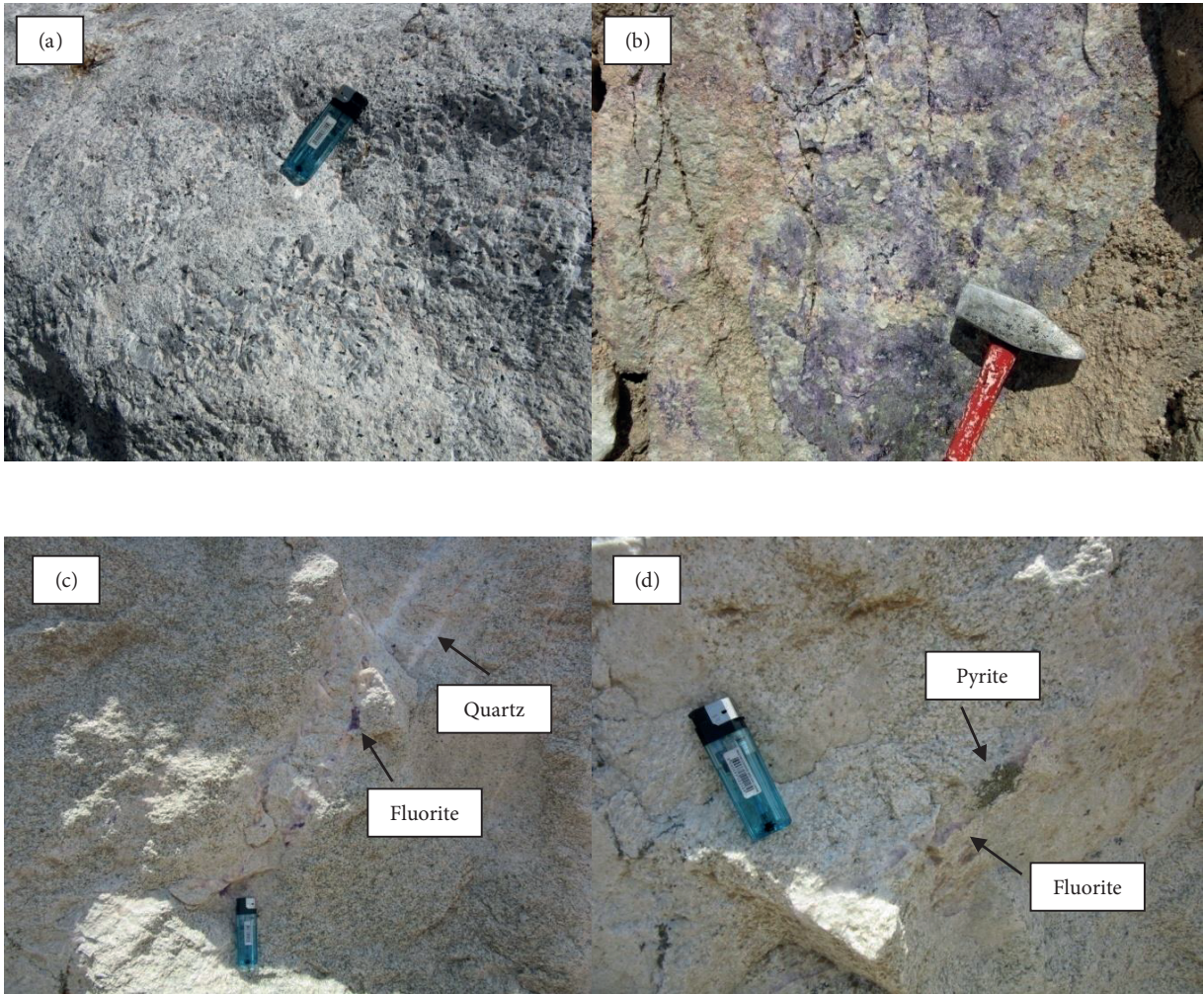
Figure 5. a) Photograph of Buzlukdağ syenite, host rock Alişar deposit; b) fluorite coatings on host rock syenite; c) quartz and fluorite association in a vein; d) pyrite formed on the wall of veins.

in previous studies (e.g., Yaman, 1985), we recognized that all the open pits had been abandoned and all that was left behind was the boulders of host rock with indistinct fluorite veins. The presence of brecciation points to unrest episodes of veins after their infill. Fluorite mostly in green color and quartz constitute the main mineral assemblage. Fluorite samples used in the present study were collected from a mine shaft that reached to a depth about 30 m.

Farther east, the Cankılı deposit is located in the Yozgat district (Figure 1). Cankılı fluorites are hosted in monzonites. Like the Akçakent deposit, the ore is mined underground at a depth of about 25 m. The veins are typically zoned; the thin quartz, less than 0.5 cm thick, makes up the central part of the vein, while multicolored fluorite occurs as layers immediately adjacent to vein walls. Calcite is the most common gangue mineral.

The Pöhrenk deposit is situated on the southern margin of the E-W extending Çiçekdağı igneous complex

(Figure 1). The complex is encircled by Upper Cretaceous ophiolites and Paleocene magmatic rocks to the north and Paleozoic metamorphic rocks of the Kırşehir Massif to the south (Şengör and Yılmaz, 1981). In the region, metamorphics are unconformably overlain by Eocene sediments with thickness of more than 100 m, which are composed of basal conglomerate, turbiditic sandstone, platform limestone, and marls interlayered with carbonate rocks (Figure 2d) (Genç, 2006). The Eocene sediments are covered by terrestrial deposits consisting of conglomerate, mudstone, and marl-siltstone. The fluorite deposits in the Pöhrenk area occur along two major NE-SW and NW-SE extending normal faults that mark the boundary between Eocene nummulitic limestones and Miocene marl-siltstone (Figure 2d). A number of pits more than 20 m across and 3–5 m in depth were opened on the foot wall of the fault at the south along the village road. Another group of pits was excavated on the hanging wall of the second fault to

the north. In the area, Eocene limestone and the overlying Miocene marl-siltstone contain various modes of fluorite mineralizations. Karstification of limestone that later silicified provided suitable open space for fluid migration and thus precipitation of ore minerals. The karstic voids are up to 1 m across and host pure coarsely crystalline euhedral yellow fluorite (Figure 6a). Collapse of karstic cavities in the limestones formed a breccia system, which is generally cemented by milky white quartz and dirty yellow fluorites (Figure 6b). Sharp orthorhombic crystals of tabular bladed barites in dull white color with length of 0.2 to 1 cm occur in a vug within the silicified limestone (Figure 6c). Brecciated zones are slightly fractured and oxidized (Figure 6d).

5. Results

5.1. Rare earth element geochemistry
Total rare earth + Y contents (ΣREY) of central Anatolian fluorites vary within a wide range from to 24 to 693

ppm (Table 2). ΣREY contents of dark purple and green fluorites are 32 to 442 ppm (average: 98 ppm; n = 13) and 89 to 693 (average: 233 ppm; n = 10), respectively. In the general sense, the chondrite-normalized REY patterns of green fluorites (Figure 7a) are slightly more flat than those of purple fluorites (Figure 7b) and the enrichment level of REY (particularly MREEs and HREEs) is almost an order of magnitude greater for the green fluorites. REY concentrations of green fluorites gently descend from La to Sm and then slightly ascend from Eu to Y and continue with a slight decrease across the HREEs. REY contents of purple fluorites also follow a similar trend with the exception that the downward trend from La to Eu is much sharper (Figure 7b). REY abundances of yellow fluorites are slightly lower than those of both purple and green fluorites and display nearly a flat pattern with a distinct positive Y anomaly (Figure 7c). Yttrium anomalies recognized in green and yellow fluorites may indicate replacement of calcium by this element (Fleischer, 1969). The apparent
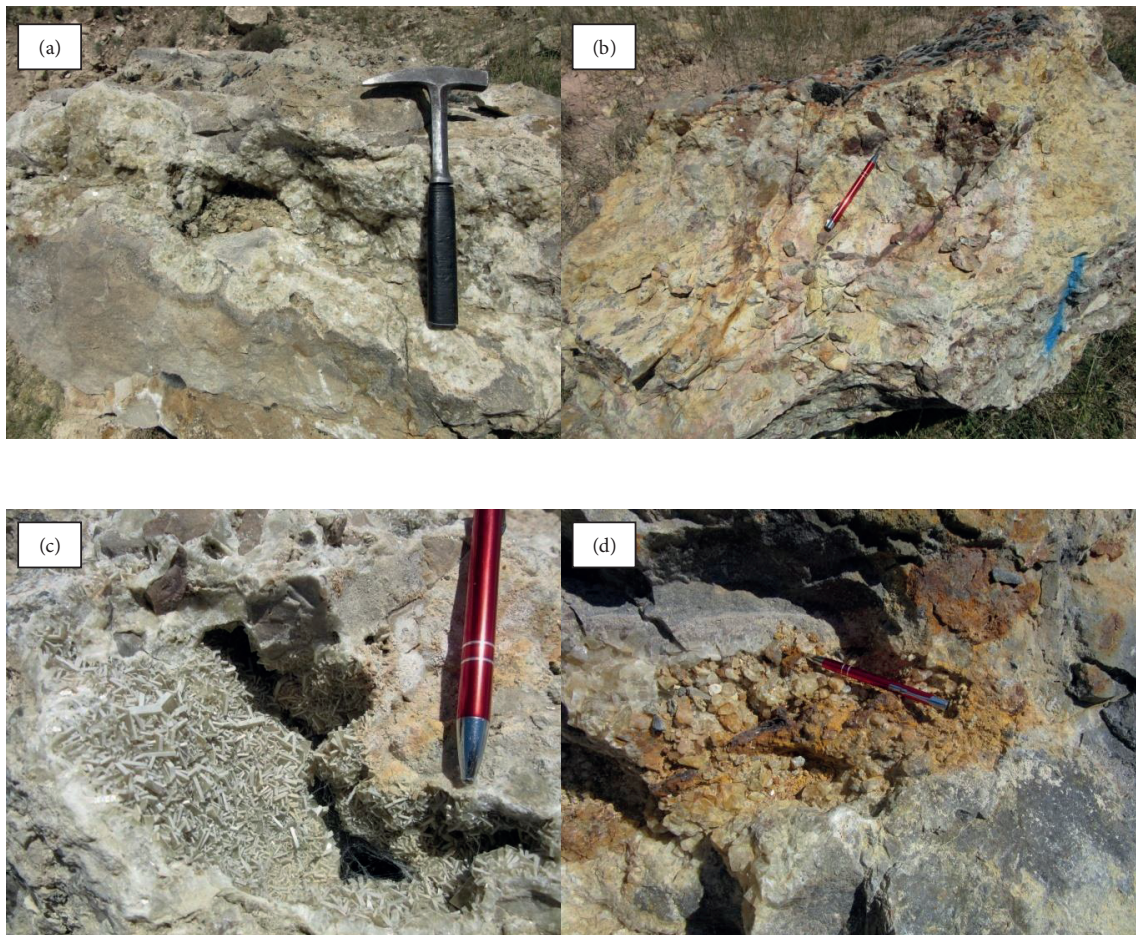

Figure 6. Various types of fluorite deposits recognized at Pöhrenk: a) coarsely crystalline fluorite crystals in karstic voids of Eocene limestone, b) brecciated host rock cemented by silica, c) orthorhombic crystals of tabular bladed barites in a vug within silicified limestone, d) slightly fractured and oxidized brecciated zones.

Table 2. REE data (including Sr and Y) for fluorite minerals and host rocks (ppm).

Fluorite type	Sample no.	Sr	La	Ce	Pr	Nd	Sm	Eu	Gd	Tb	Dy	Y	Ho	Er	Tm	Yb	Lu	ΣREE + Y	Eu/Eu*	Ce/Ce*
Dark purple	BYD1-1/1	235.1	22.8	39.2	3.48	12.6	3.65	1.27	5.94	1.29	8.60	69.7	1.75	5.32	0.71	4.38	0.57	181.3	0.83	1.06
	BYD1-1/21	238.0	6.2	9.8	0.82	3.0	0.89	0.35	1.67	0.36	2.52	18.0	0.48	1.62	0.21	1.34	0.18	47.4	0.88	1.05
	BYD2-1/1	236.1	4.1	5.7	0.61	2.5	0.52	0.31	1.28	0.30	2.14	14.1	0.41	1.36	0.15	1.06	0.18	34.7	1.16	0.87
	BYD3-1	237.9	12.6	9.2	1.53	5.3	0.83	0.21	1.01	0.20	1.11	10.4	0.19	0.75	0.10	0.59	0.09	44.1	0.70	0.51
	BYD-3/1	244.3	12.7	19.4	1.82	5.2	1.23	0.39	1.95	0.43	3.21	22.5	0.60	1.73	0.25	1.70	0.25	73.4	0.77	0.98
	BYD-4/1	183.0	6.0	8.7	0.84	3.1	0.55	0.21	0.98	0.23	1.51	11.2	0.31	0.95	0.14	1.05	0.14	35.9	0.87	0.94
	BYD-4/2	210.2	6.7	12.8	0.72	1.7	0.24	0.07	0.59	0.11	0.81	6.8	0.12	0.36	0.06	0.31	0.04	31.4	0.57	1.41
	BYD-5/1	230.9	11.9	18.1	1.58	5.3	0.95	0.40	1.66	0.36	2.26	14.2	0.43	1.14	0.18	1.24	0.16	59.9	0.97	1.01
	BYD-6	288.6	18.6	30.7	2.26	7.3	0.71	0.17	0.77	0.10	0.49	2.2	0.11	0.22	0.03	0.17	0.03	63.9	0.70	1.15
	ISA-3	144.8	14.3	20.9	3.00	12.0	2.46	0.68	2.16	0.36	2.02	12.1	0.27	0.73	0.08	0.54	0.06	71.7	0.90	0.77
	ALI-3/2	659.0	11.2	19.7	2.49	11.9	2.08	0.55	1.90	0.22	0.90	21.8	0.19	0.43	0.05	0.26	0.05	73.7	0.84	0.90
	ALI-4	977.7	109.8	178.3	17.67	59.7	7.66	1.51	6.21	0.70	3.78	50.8	0.77	2.16	0.30	1.85	0.24	441.5	0.67	0.98
	AKC-1/1	84.5	10.0	20.7	2.31	9.1	2.06	0.79	3.41	0.79	5.25	51.9	1.21	3.83	0.65	4.60	0.62	117.2	0.91	1.04
Green	BYD2-1/2	323.9	18.5	35.0	4.17	18.8	7.34	3.14	13.89	2.99	21.04	156.3	4.36	13.23	1.73	10.57	1.38	312.4	0.95	0.96
	BYD1-1/22	313.8	18.0	32.4	3.94	17.7	7.02	3.14	13.71	2.95	19.94	150.9	4.30	12.81	1.68	10.14	1.41	300.0	0.98	0.93
	BYD3-2	327.2	20.7	35.5	4.28	17.6	7.04	3.13	13.72	2.94	20.52	149.1	4.51	12.54	1.70	10.31	1.38	305.0	0.97	0.91
	BYD-5/2	378.6	24.5	57.4	7.68	40.8	18.82	7.90	35.31	7.29	48.58	372.0	10.15	29.09	4.07	25.86	3.34	692.8	0.93	1.01
	AKC-1/2	76.5	4.7	10.8	1.21	5.5	1.22	0.52	2.39	0.54	3.60	52.0	0.80	2.58	0.37	2.05	0.26	88.5	0.93	1.10
	AKC-1/3	55.5	2.9	5.9	0.84	3.7	0.98	0.47	2.21	0.49	3.90	63.3	0.88	2.58	0.35	2.18	0.27	91.0	0.97	0.91
	AKC-2/1	165	17.5	38.8	5.02	19.6	4.35	1.17	4.36	0.73	4.44	34.7	0.78	2.50	0.40	2.41	0.31	137.1	0.82	1.00
	AKC-2/2	81.7	4.7	11.5	1.54	5.7	1.77	0.75	3.34	0.76	5.02	70.5	1.15	3.25	0.47	3.19	0.41	114.1	0.94	1.03
	AKC-6	71.8	4.0	9.7	1.59	8.5	3.41	1.84	6.63	1.25	6.48	73.4	1.18	2.79	0.32	1.56	0.20	122.9	1.18	0.93
	CAN-1	304.5	9.1	23.8	3.45	16.4	6.29	2.64	8.83	1.84	11.81	67.2	2.45	7.22	1.15	7.53	1.14	170.9	1.08	1.03
Yellow	PHR-1/1	43.4	1.2	2.2	0.37	2.2	0.69	0.26	1.12	0.19	1.17	16.8	0.21	0.49	0.05	0.35	0.03	27.3	0.90	0.80
	PHR-2/1	41.9	1.4	2.5	0.39	2.1	0.66	0.27	1.07	0.18	1.03	17.3	0.20	0.60	0.06	0.25	0.04	28.1	0.98	0.82
	PHR-2/2	104.5	0.8	2.3	0.31	2.0	0.66	0.14	1.21	0.18	1.16	13.8	0.22	0.51	0.07	0.43	0.06	23.9	0.48	1.12
Calcite	ALI-3/1	2076.6	194.6	295.0	30.63	98.1	10.48	2.10	7.25	0.71	3.30	20.3	0.53	1.52	0.21	1.49	0.24	666.5	0.73	0.92
Limestone	PHR-10/2	8.4	0.5	0.5	0.09	0.3	0.06	0.03	0.12	0.02	0.15	1.4	0.02	0.07	0.01	0.05	0.01	3.3	1.08	0.57
Syenite	ALI-10	419.1	251.4	406.7	37.53	98.8	7.06	0.88	2.33	0.16	0.57	3.9	0.06	0.20	0.04	0.32	0.06	810.0	0.66	1.01
Syenite	BYD-10	65.6	100.9	150.8	11.55	27.6	2.83	0.37	1.65	0.23	1.18	9.0	0.22	0.87	0.15	1.21	0.20	308.8	0.52	1.06
Monzonite	CAN-10	1115.3	55.9	99.8	10.91	37.7	6.48	1.74	5.11	0.73	3.84	19.8	0.72	2.13	0.31	1.98	0.29	247.4	0.92	0.98
Syenite	AKC-10	298.3	172.2	210.6	17.27	44.2	5.38	1.04	4.34	0.52	2.85	18.8	0.54	1.84	0.30	2.38	0.38	482.6	0.65	0.93
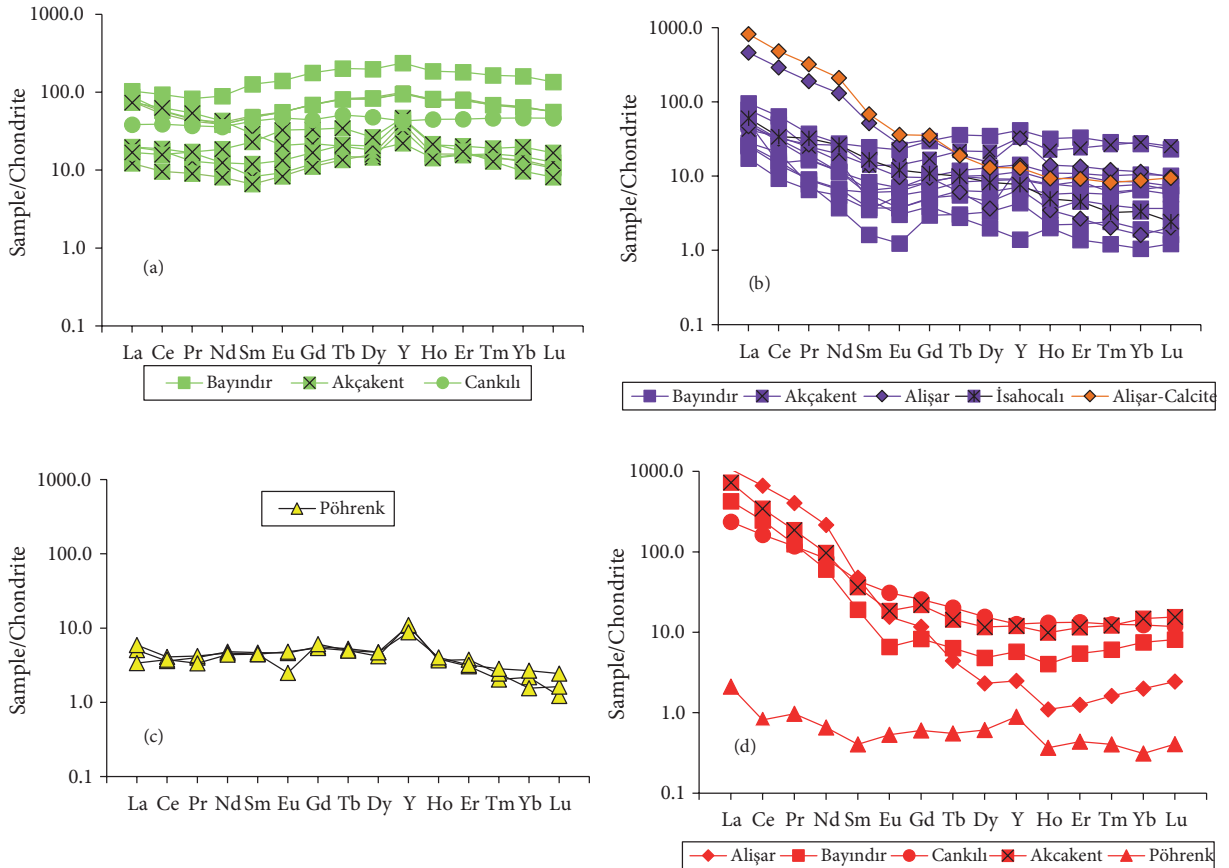
Figure 7. Chondrite normalized (McDonough and Sun, 1995) REY patterns: a) green fluorites, b) dark purple fluorites, c) yellow fluorites, d) host rocks.

difference in the degree of enrichment of REY contents may indicate that fluorites of all colors were precipitated from different hydrothermal fluids.

LREE contents of host rocks are significantly higher than all fluorite types (Figure 7d). Samples from Bayındır (BYD-10), Cankılı (CAN-10), Akçakent (AKC-10), and Buzlukdağ (ALI-10) magmatic rocks are represented by ΣREY concentrations notably greater than fluorites except for Pöhrenk limestone (PHR-10/2), which has the lowest REY content among the whole dataset. Yellow fluorites collected from the Pöhrenk deposit clearly imprint the REY-depleted character of host limestones in this region (Figures 7c and 7d). One calcite sample collected from the Alişar deposit generally follows the same trend as the host rocks (Figure 7b). It is clear from REY data that the source of the hydrothermal solution, which formed the fluorite mineralizations, cannot be a simple leaching from host magmatic rocks.

5.2. Fluid inclusion studies

Microthermometric measurements were conducted on a total of 191 primary, secondary (occurring mostly along the crystal growth zones), and pseudosecondary inclusions hosted in fluorite. The results are summarized in Table 3 and shown as histograms in Figure 8. Primary inclusions in fluorites are irregularly shaped, cubic, rectangular, or tabular. The secondary inclusions have rounded or oval shapes (Figures 9a–9c). Inclusions have lengths varying in a wide range from 5 to 140 μm and rarely show a necking-down structure.

Except for a small number of Pöhrenk samples, which homogenized into the vapor phase, the vast majority of inclusions (~98%) homogenized into the liquid phase upon heating. The ice-melting temperatures (Tm-ice) were converted to salinity using data for the H_2O-NaCl system (Bodnar, 1993). The studied inclusions contain no solid phase (salt or daughter mineral) and no sign of boiling was recognized. In all the samples, inclusions are two-phase (L-V) at room temperature (Figure 9d).

For the Bayındır, Yeniyapan, İsahocalı, and Alişar deposits, measurements were carried out on primary (n = 67) and pseudosecondary (n = 18) inclusions in fluorite (green and purple), which yielded a wide range of homogenization temperatures of 95 to 205 °C and 102 to 181 °C, respectively. The majority of inclusions from

Table 3. Results of microthermometric measurements of fluorite minerals.

Deposit	Sample No.	Fluorite color	FI type	Temp. of first ice melting (Te) (°C)	Temp. of final ice melting (Tm-ice) (°C)	Homogenization temp. (Th) (°C)	Hom. phase	Salinity (wt.% NaCl equiv.)
Bayındır	BYD-D1	Purple	P (5)	−43 to −31 (4)	−2.4 to −0.9 (5)	131 to 150 (5)	L (5)	0.5 to 4 (5)
	BYDl.2	Purple	P (3)	−39 to −38 (3)	−4.9 to −1.3 (3)	171 to 175 (3)	L (3)	2.2 to 7.7 (3)
			PS (9)	−35 to −20 (9)	−2.7 to 0 (9)	102 to 132 (9)	L (9)	0 to 4.5 (9)
	BYD-D2	Purple	P (4)	−46 to −30 (4)	−4.8 to −1.4 (4)	126 to 173 (4)	L (4)	2.4 to 7.6 (4)
		Green	P (8)	−49 to −38 (5)	−2.9 to −0.1 (8)	146 to 191 (8)	L (8)	0.2 to 4.8 (8)
	BYD3.1	Purple	P (3)	−35 to −26 (3)	−4.4 to −0.2 (3)	152 to 158 (2)	L (2)	0.4 to 7 (3)
	BYD3/1	Purple	P (3)	−40 to −22 (2)	−6.8 to −0.8 (3)	118 to 178 (2)	L (2)	1.4 to 10.2 (3)
	BYD4/1	Purple	P (3)	−42 to −28 (3)	−4 to −2 (3)	102 to 122 (3)	L (3)	3.7 to 6.5 (3)
	BYD-7	Purple	P (3)	−40 to −30 (2)	−8 to −3.2 (2)	95 to 191 (3)	L (3)	5.3 to 11.7 (2)
			PS (3)	−42 to −22 (8)	−4.3 to −0.7 (8)	120 to 181 (8)	L (8)	1.2 to 6.9 (8)
	BYD-6	Purple	PS (4)	−44 to −18 (4)	−9.9 to −1 (4)	107 to 143 (4)	L (4)	1.7 to 13.8 (4)
			P (4)	−41 to −33 (4)	−5.2 to −1 (4)	155 to 200 (4)	L (4)	1.7 to 8.1 (4)
	BYD-D6	Purple	PS (2)	−37 to −34 (2)	−5 to −1.5 (2)	102 to 112 (2)	L (2)	2.6 to 7.9 (2)
İsahocalı	İSA-1	Purple	P (4)	−41 to −28 (3)	−2.8 to −0.3 (4)	116 to 158 (4)	L (4)	0.5 to 4.7 (4)
	İSA-3	Purple	P (11)	−48 to −22 (11)	−4 to 0 (11)	120 to 205 (11)	L (11)	0 to 6.5 (11)
Alişar	ALI-1	Purple	P (16)	−48 to −24 (13)	−7.4 to 0 (16)	111 to 210 (16)	L (16)	0 to 12.3 (16)
	AKC-6.1	Green	P (6)	−46 to −28 (6)	−3 to 0 (6)	168 to 209 (6)	L (6)	0 to 5 (6)
			PS (8)	−44 to −22 (8)	−2.1 to 0 (8)	147 to 218 (8)	L (8)	0 to 3.6 (8)
Akçakent	AKC-6.2	Green	P (7)	−44 to −27 (7)	−8 to 0 (7)	148 to 240 (7)	L (7)	0 to 11.7 (7)
			PS (3)	−33 to −27 (3)	−5 to −3 (3)	150 to 172 (3)	L (3)	5 to 7.9 (3)
Cankılı	CAN-1	Green	P (11)	−43 to −30 (11)	−1.5 to 0 (11)	150 to 178 (11)	L (11)	0 to 2.6 (11)
			PS (9)	−55 to −33 (9)	−2 to 0 (9)	145 to 198 (9)	L (9)	0 to 3.4 (9)
	CAN-2	Green	PS (6)	−38 to −24 (6)	−3.8 to −0.6 (5)	161 to 190 (6)	L (6)	1.1 to 6.2 (5)
			S (4)	−27 to −25 (2)	−0.7 to 0 (2)	142 to 182 (4)	L (4)	0 to 1.2 (2)
			P (6)	−32 to −20 (4)	0 (4)	128 to 188 (6)	L (6)	0 (4)
	PHR-V	Yellow	P (11)	−39 to −22 (11)	−11 to 0 (11)	120 to 265 (11)	L (11)	0 to 15 (11)
			P (2)	−33 (2)	−13 to −5 (2)	213 to 248 (2)	V (2)	7.9 to 16.9 (2)
			PS (2)	−34 to −27 (2)	−9 to −4 (2)	117 to 130 (2)	L (2)	6.5 to 12.9 (2)
			S (4)	−36 to −31 (4)	−6.5 to −1.4 (4)	86 to 153 (3)	L (3)	2.4 to 9.9 (4)
	PHR-23	Yellow	P (14)	−45 to −28 (14)	−16.7 to −1 (13)	99 to 276 (11)	L (11)	1.7 to 20 (13)
Pöhrenk			PS (3)	n.d.	−3.2 to −3 (3)	123 to 133 (3)	L (3)	5 to 5.3 (3)
	PHR-24	Yellow	P (12)	−45 to −30 (11)	−6.5 to −1.5 (11)	135 to 235 (10)	L (10)	2.6 to 9.9 (11)
				−34 (1)	−3 (1)	292 (1)	V (1)	5 (1)

P: Primary, S: secondary, PS: pseudosecondary inclusions, n.d.: not determined. Number of measurements is given in parentheses.
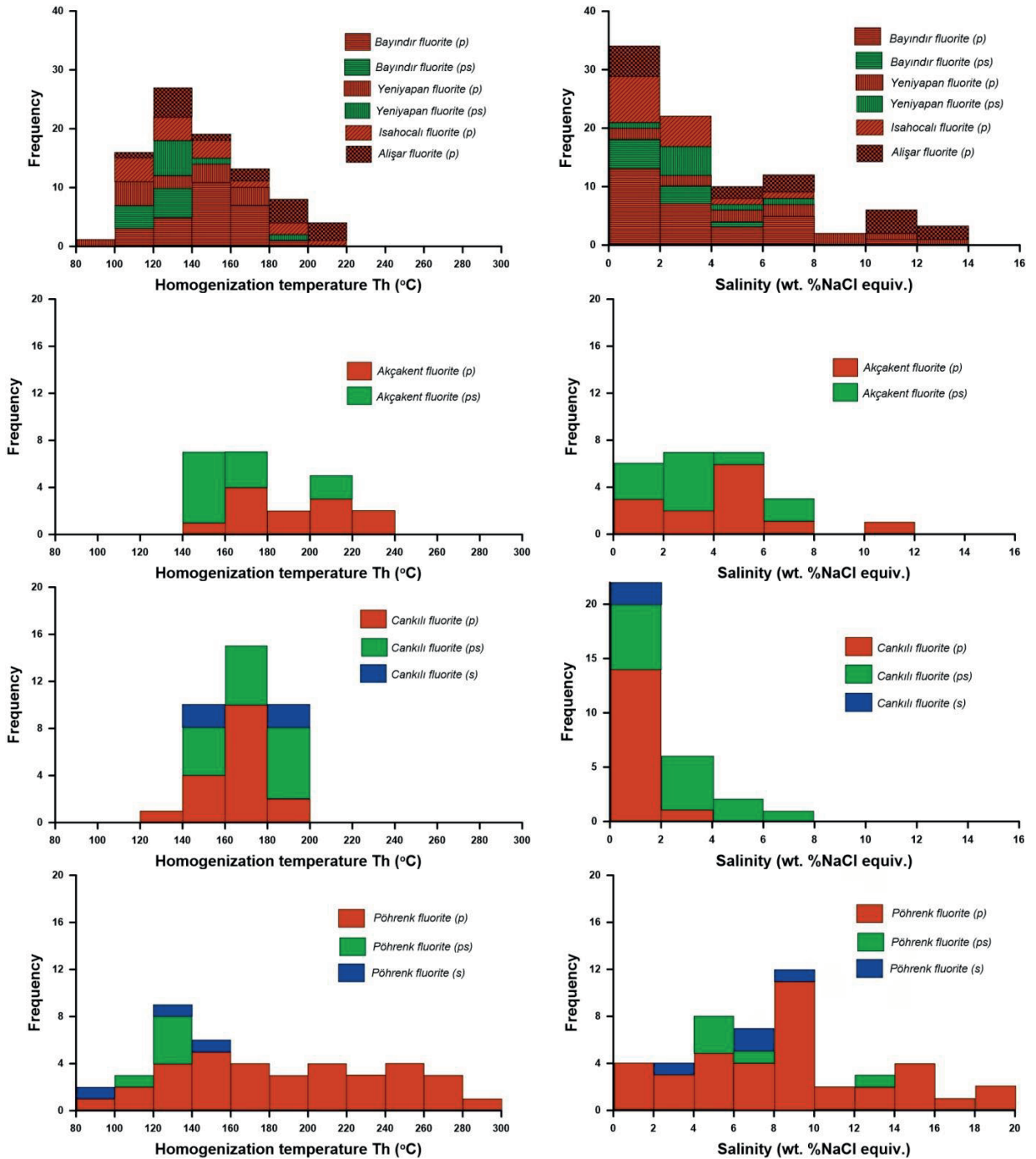
Figure 8. Histograms for homogenization temperatures and salinities of primary (p), secondary (s), and pseudosecondary (ps) fluid inclusions within fluorites.

the Bayındır fluorites were distributed at 120–180 °C, although populations with lower (80–120 °C) and higher temperatures (180–220 °C) from the Alişar, İsahocalı, and Yeniyapan fluorites were also recorded. Salinities of primary inclusions from the Bayındır fluorites are in the range of 0 to 12 wt.% NaCl equiv., whereas Alişar and

Yeniyapan inclusions have salinities up to 14 wt.% NaCl equiv (Table 3; Figure 8). The decrease in Th values shows cooling of mineralizing fluid.

Regarding the Akçakent deposit, measurements were carried out on both primary (n = 13) and pseudosecondary (n = 11) inclusions trapped only in green fluorite.
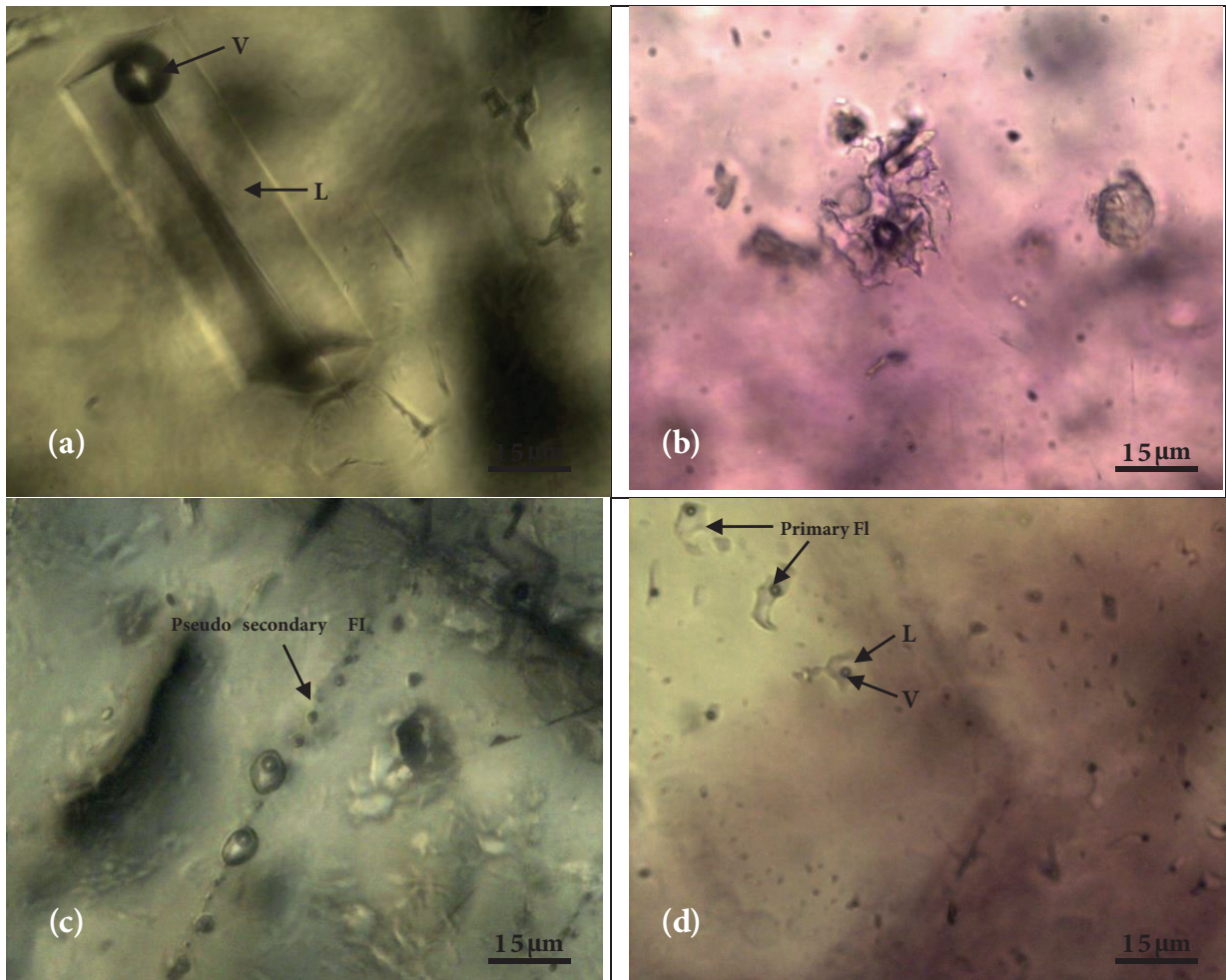
Figure 9. Photomicrographs of fluid inclusions (taken at room temperature): a) a cubic two-phase primary fluid inclusion in fluorite, b) irregular two-phase primary inclusion in fluorite, c) pseudosecondary two-phase inclusions in fluorite, d) primary two-phase inclusions in fluorite. FI = Fluid inclusion; L = liquid; V = vapor.

Homogenization temperatures of the inclusions vary in a wide range from 147 to 240 °C. The last ice melting temperatures are within the range of –8 to 0 °C, which estimates salinities of 0 to 11.7 wt.% NaCl equiv. These values are slightly lower than the upper range of the Bayındır inclusions (14 wt.% NaCl equiv.).

For the Cankılı deposit, fluid inclusion measurements were conducted on primary (n = 17), secondary (n = 4), and pseudosecondary (n = 15) inclusions hosted in green fluorites. Inclusions were homogenized into liquid phase at temperatures in the range of 128 to 198 °C. Excluding only one measurement, the homogenization temperatures of inclusions do not exceed 200 °C (Table 3; Figure 8). Low homogenization temperatures of inclusions are accompanied by low salinities ranging from 0 to 6.2 wt.% NaCl equiv.

Fluid inclusion measurements for the Pöhrenk deposit were carried out on primary (n = 39), secondary (n = 4),

and pseudosecondary (n = 5) inclusions in yellow fluorites. Homogenization temperatures of primary inclusions vary in a broad range (99 to 292 °C) and are greater than those of both secondary (86 to 153 °C) and pseudosecondary (117 to 133 °C) inclusions. Salinities estimated are also in a wide range from 5 to 12.9 wt.% NaCl equiv. for pseudosecondary inclusions, 2.4 to 9.9 wt.% NaCl equiv. for secondary inclusions, and 0 to 20 wt.% NaCl equiv. for primary inclusions (Table 3; Figure 6). Among the studied fluorites, high homogenization temperatures (up to 292 °C) recorded for primary inclusions from Pöhrenk fluorites are consistent with the data of Uras (2007) (78 to 363 °C) but lower than temperatures reported by Genç (2006) (58 to 154 °C).

5.3. Sr-Nd isotope data
Sr concentrations of dark purple fluorites are within the range of 85 to 978 ppm (average: 305 ppm), whereas those of green fluorites vary from 56 to 379 ppm (average: 210

ppm). Yellow fluorites have the lowest Sr contents with an average of 63 ppm (Table 2). Host rocks of each deposit, except for the Bayındır area, have slightly higher Sr concentrations.

$^{87}Sr/^{86}Sr$ values of fluorite samples vary in a narrow range from 0.707627 to 0.709380 (Table 4). One calcite sample from the Alişar deposit ($^{87}Sr/^{86}Sr$ = 0.707916) and host rocks from the Alişar ($^{87}Sr/^{86}Sr$ = 0.708783) and Cankılı ($^{87}Sr/^{86}Sr$ = 0.709733) areas were also analyzed for comparison. Sr isotope compositions do not show a systematic variation among fluorites of different colors. Only one yellow fluorite sample from the Pöhrenk deposit (0.707627) and two purple fluorite samples from Alişar (0.708232 and 0.707832) yielded the lowest $^{87}Sr/^{86}Sr$ ratios. The host monzonite from Cankılı has the highest Sr isotope composition (0.709733) in the entire dataset. Kadıoğlu and Deniz (2015) recently reported $^{87}Sr/^{86}Sr$ values of 0.69799–0.70218 and 0.68727–0.69517 from purple and green fluorites from Bayındır, respectively.

A moderate correlation exists between $^{87}Sr/^{86}Sr$ and 1/Sr (ppm) values (Figure 10a). It is noticeable that Sr isotope

compositions of host rocks from the Alişar and Cankılı areas are within the range of fluorite samples. However, Sr concentrations of syenite and calcite samples from the Alişar area are noticeably higher than those of fluorites.

Nd isotope analysis was conducted on a limited number of fluorite samples only from the Bayındır deposit. $^{143}Nd/^{144}Nd$ values of samples fall in a narrow range from 0.512366 to 0.512681 (Table 4). Unlike Sr isotopes, Nd isotope ratios display two distinct clusters: green fluorites are represented by higher $^{143}Nd/^{144}Nd$ values (0.512676 to 0.512681) than the purple fluorites (0.512366 to 0.512548) (Figure 10b). Similarly, Nd concentrations of the two datasets are also different. Dark purple fluorites have lower Nd contents (1.7 to 12.6 ppm) compared to green fluorites (17.6 to 18.8 ppm; Table 2).

5.4. Stable isotopes

Stable isotope compositions of various minerals occurring in fluorite deposits are presented in Table 5. $\delta^{18}O$ values of quartz from the Bayındır, Yeniyapan, and Akçakent deposits vary from 10.6‰ to 15.4‰ (vs. VSMOW). $\delta^{13}C$ and $\delta^{18}O$ values of calcites collected from the Alişar and

Table 4. Sr-Nd data for central Anatolian fluorite deposits.

Fluorite type	Sample no.	$^{87}Sr/^{86}Sr$	$^{134}Nd/^{144}Nd$
Dark purple	BYD1-1/1	0.709240 ± 25	0.512536 ± 04
	BYD1-1/21	0.708857 ± 11	0.512539 ± 21
	BYD2-1/1	0.708678 ± 08	0.512548 ± 24
	BYD3-1	0.708894 ± 14	0.512374 ± 05
	BYD-3/1	0.708993 ± 18	0.512396 ± 4
	BYD-4/1	0.708654 ± 12	0.512406 ± 13
	BYD-4/2	0.709380 ± 23	0.512366 ± 14
	BYD-5/1	0.708682 ± 12	n.a.
	BYD-6	0.708675 ± 13	n.a.
	ISA-3	0.709030 ± 15	n.a.
	ALI-3/2	0.708232 ± 19	n.a.
	ALI-4	0.707832 ± 12	n.a.
Green	BYD2-1/2	0.708888 ± 19	0.512676 ± 04
	BYD1-1/22	0.708975 ± 21	0.512681 ± 04
	BYD3-2	0.709266 ± 18	0.512678 ± 03
	BYD-5/2	0.708286 ± 17	n.a.
	AKC-2/1	0.709237 ± 29	n.a.
	CAN-1	0.708248 ± 27	n.a.
Yellow	PHR-2/2	0.707627 ± 26	n.a.
Calcite	ALI-3/1	0.707916 ± 07	n.a.
Syenite	ALI-10	0.708783 ± 19	n.a.
Monzonite	CAN-10	0.709733 ± 05	n.a.
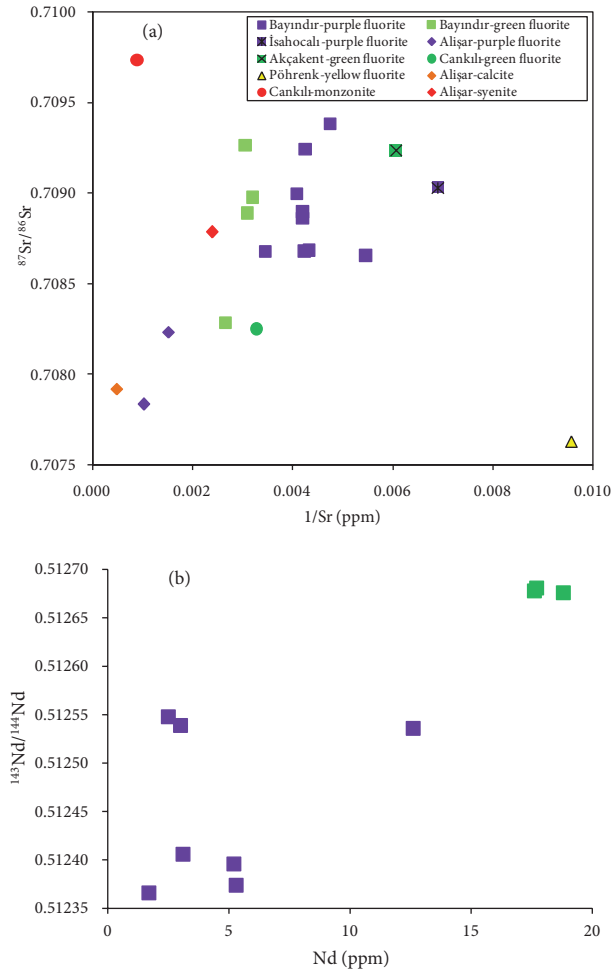
Figure 10. a) $^{87}Sr/^{86}Sr$ vs. 1/Sr (ppm) diagram for fluorite and host rock samples (red circles); b) $^{143}Nd/^{144}Nd$ vs. Nd (ppm) diagrams for Bayındır fluorite samples.

Cankılı areas are –3.22‰ to –0.39‰ (vs. VPDB) and 9.87‰ to 13.05‰ (vs. VSMOW), respectively. According to Genç (2006), the carbon isotope composition of fluid inclusion waters from the Pöhrenk fluorite deposit are –41.7‰ to –36.0‰ (vs. SMOW) and δD-δ^{18}O values are in the range of –42‰ to –33‰ and –6.1‰ to –2.5‰, respectively.

Oxygen isotope compositions of quartz are slightly greater than the magmatic range proposed by Taylor (1967). Carbon isotope compositions of calcites are within the range of marine carbonates (–3‰ to +3‰: Hoefs, 1987; Clark and Fritz, 1997). δ^{18}O values of calcite samples are slightly higher than the magmatic source but significantly lower than marbles (~30‰; Bowman et al., 1985), which may be attributed to continuous prograde reactions in the country rocks promoted by pluton-derived fluids (e.g., Orhan et al., 2011).

δ^{34}S values of pyrites (–2.9‰ to 0.2‰; VCDT) from the Alişar and Akçakent deposits indicate a magmatic origin (~0‰). On the other hand, sulfur in barites collected from the Pöhrenk deposit shows diverse compositions. The δ^{34}S of sample PHRB1 (20.3‰) most probably signifies a marine source (10‰ to 35‰; Clark and Fritz, 1997), whereas the sulfur isotopic composition of sample PHRB2 (5.5‰) may be explained by a mixing of sulfur from marine and terrestrial sources (–15‰ to 10‰; Clark and Fritz, 1997).

6. Discussion

6.1. Significance of REE data

Fluorite is one of the best minerals to examine REE fractionation in fluorine-rich hydrothermal solutions (Bau and Dulski, 1995). Fractionation of REEs could be tested using various diagrams based on REE ratios. Yttrium, as a pseudolanthanide, behaves in a similar manner as holmium since the ionic radii of these elements are very similar and both occur in the trivalent oxidation state. If REEs in a sample are not fractionated, the Y/Ho and La/Ho ratios should be constant. On the contrary, cogenetic fluorites that are not precipitated simultaneously may yield a negative correlation between Y/Ho and La/Ho. Y/Ho ratios of central Anatolian fluorites (from 20 to 115), except for two samples, are higher than the chondritic ratio of 28 (Bau and Dulski, 1995) (Figure 11a). Variation in La/Ho is almost two orders of magnitude greater than that for Y/Ho, which is attributed to either crystallization of a LREE-enriched phase in the hydrothermal system or partial removal of a LREE-enriched phase during the fluorite formation. Furthermore, positive Y anomalies recognized in most of samples indicate Y-Ho fractionation, which is probably not a source-related event but mostly depends on fluid composition. It is noticeable that the studied fluorites comprise two groups: green fluorites with a LREE-enriched pattern and purple fluorites with a LREE-depleted pattern. Yellow fluorites from the Pöhrenk deposit with low La/Ho ratios also accompany the green fluorites (Figure 11a).

According to Möller et al. (1981), Tb/Ca and Tb/La ratios are very helpful to depict various steps of fluorite crystallization. In Figure 11b, both the Tb/Ca and the Tb/La of samples show an increasing trend, indicating a progressive REE fractionation with fluorite formation. Therefore, lower points correspond to early stages of mineralization whereas upper points with higher fractionation represent the late stage. Regarding Tb/Ca and Tb/La ratios, all fluorite samples except one are distributed in the hydrothermal field. Samples from the Pöhrenk deposit are plotted close to the boundary between hydrothermal and sedimentary fields since the Pöhrenk mineralization formed in a sedimentary environment. In

Table 5. Stable isotope compositions of gangue minerals (‰) in central Anatolian fluorite deposits.

Deposit	Sample no.	Mineral	$\delta^{18}O$ (VSMOW)	$\delta^{13}C$ (VPDB)	$\delta^{34}S$ (VCDT)
Bayındır	BYDS1	Quartz	14.30		
Yeniyapan	BYDS5	Quartz	15.40		
Akçakent	AKCS1	Quartz	10.60		
Akçakent	AKCS6	Quartz	13.50		
Alişar	ALIC3	Calcite	13.05	−3.22	
Cankılı	CANC1	Calcite	9.87	−0.39	
Akçakent	AKCP1	Pyrite			0.2
Alişar	ALIP1	Pyrite			−2.9
Pöhrenk	PHRB1	Barite			20.3
Pöhrenk	PHRS2	Barite			5.5

Figure 11b, samples are categorized into subgroups: purple fluorites (more pronounced for Bayındır samples), which crystallized at the beginning of mineralization, and green fluorites, which precipitated in a later phase. Akçakent and Pöhrenk fluorites with an almost parallel trend in Tb/La and a constant position in Ta/Ca are indicative of secondary crystallization. During remobilization of fluorite, all HREEs stay in solution whereas mobile elements (e.g., La) undergo ion exchange with solid phases (Möller et al., 1976).

Among the REEs, Ce and Eu occurring in multiple valences yield information on the oxidation state of mineralizing fluids. Reduction of Eu^{3+} to Eu^{2+} under euxinic conditions at temperatures exceeding 250 °C results in positive Eu anomalies and oxidation of Ce under high oxygen fugacities produces negative Ce anomalies since Ce^{4+} is adsorbed on oxyhydrates (Möller et al., 1981). Eu/Eu* and Ce/Ce* ratios of central Anatolian fluorites, computed to estimate the magnitude of the Ce and Eu anomalies (Taylor and McLennan, 1985), vary in a wide range from 0.48 to 1.18 and 0.51 to 1.41, respectively (Table 2). If these ratios are assessed with respect to the color of fluorites, green fluorites (Eu/Eu* = 0.82 to 1.18 and Ce/Ce* = 0.91 to 1.10) are found to have a narrow range compared to purple fluorites (Eu/Eu* = 0.57 to 1.16 and Ce/Ce* = 0.51 to 1.41). All but only three of the samples show negative Eu anomalies. This may imply the existence of Eu^{2+} and low oxygen fugacities. In other words, Eu did not substantially substitute Ca in fluorite. Unlike Eu, half of the fluorite samples are represented by negative Ce anomalies. This indicates that both high and low oxidizing conditions prevailed at an equal rate at the site of crystallization. Any Ca-bearing mineral such as calcite, which precipitated from mineralizing fluid, could result in a negative Ce anomaly. On the other hand, a positive Ce anomaly in

samples might be attributed to two processes (Sánchez et al., 2010): the Ce content of the fluids was already Ce^{3+}-enriched prior to fluorite formation (inherited anomaly) and reduction of Ce^{4+} to Ce^{3+} at the site of deposition, increasing the Ce content of fluid to be incorporated into fluorite.

6.2. The source of mineralizing fluid
Homogenization temperatures measured in fluorites vary in a wide range from 86 to 292 °C with an average of 165 °C, indicating a low-temperature array for hydrothermal solutions. The highest temperatures and salinities recorded from yellow fluorites from Pöhrenk might be due to the deeper circulation of hydrothermal waters.

Oxygen isotope data on quartz minerals collected from the Bayındır and Akçakent fluorite veins can be used to estimate the $\delta^{18}O$ value of mineralizing fluid. Assuming a temperature value of 200 °C for the vein growth (since quartz controls the silica saturation at temperatures greater than 180 °C; Fournier, 1991), fluid in equilibrium with quartz is found to have oxygen isotope composition varying from −1.6‰ to 3.2‰ (Clayton et al., 1972). These values, even at the upper limit of the calculated range, are significantly lower than those proposed for magmatic waters (e.g., Taylor, 1978) and also slightly higher than meteoric waters. This may be attributed to the interaction of surface-derived fluids with ^{18}O-enriched rocks at moderate temperatures under hydrothermal conditions. According to Genç (2006), $\delta^{18}O$ values of fluid inclusion waters measured in fluorites from the Pöhrenk deposit vary from −6.1‰ to −2.5‰, which are close to the central Anatolia meteoric water line and slightly overlap with the oxygen isotope composition of formation waters (Sheppard, 1994). Variation in $\delta^{18}O$ values might explain the presence of multiphase precipitation in the veins. The sulfur isotope composition of pyrites in the Akçakent and
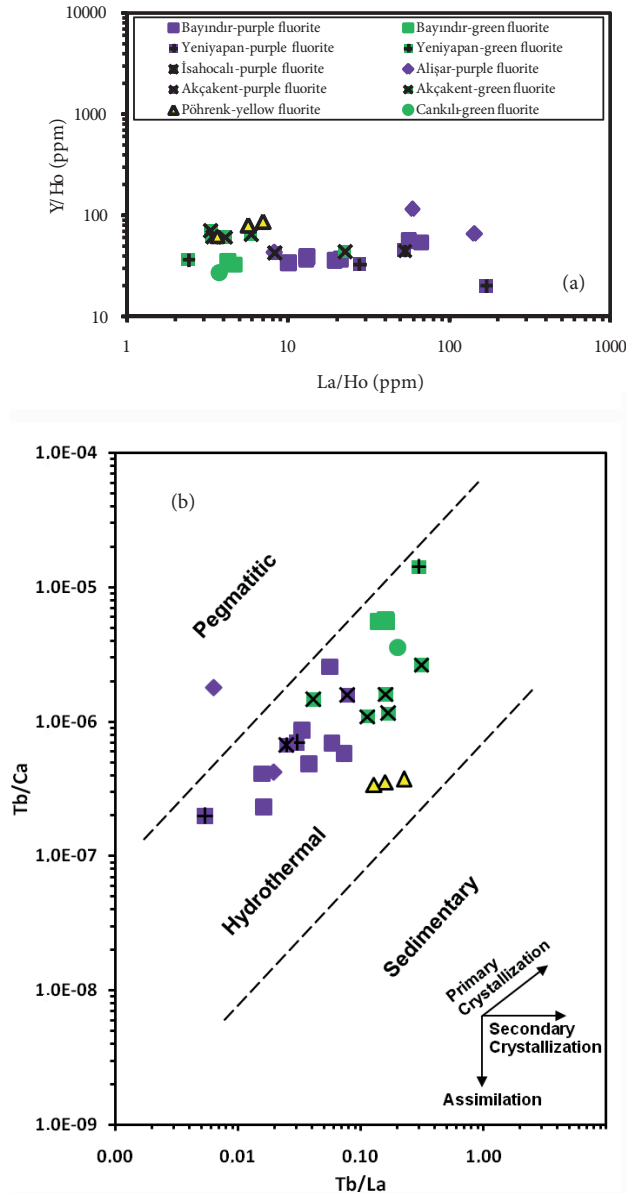
Figure 11. a) Y/Ho vs. La/Ho (Bau and Dulski, 1995) and b) Tb/Ca vs. Tb/La (Möller et al., 1981) diagrams for the samples.

Alişar deposits falls in the magmatic range. This clearly indicates that the mineral precipitation in these areas was contributed by a distinct pulse of magmatic fluids.

The Sr-Nd isotope systematics of the Bayındır fluorite samples are conformable with that of the Bayındır syenite (Ilbeyli et al., 2004) (Figure 12). This may imply that hydrothermal fluids progressively reacted with the host syenite until they became entirely equilibrated. There may also be a possibility that the Sr in mineralizing fluids and Bayındır syenite originated from a similar source region. However, these arguments cannot be tested for other fluorite deposits since Sr-Nd isotope data are not available.

The homogeneous $^{143}Nd/^{144}Nd$ values of the samples indicate that fluids were equilibrated with the host rock through dissolution-precipitation and isotope exchange reactions. Given that the equilibration rate of Nd is slower than that of Sr, the observed Sr-Nd isotope systematics may imply that there was sufficient time for the equilibrium to proceed. If this is the case, studied fluorite veins had to be precipitated in a long period of time after the syenite emplacement. However, this does not rule out the possibility that mineralizing fluids and Bayındır syenite were derived from a similar source.
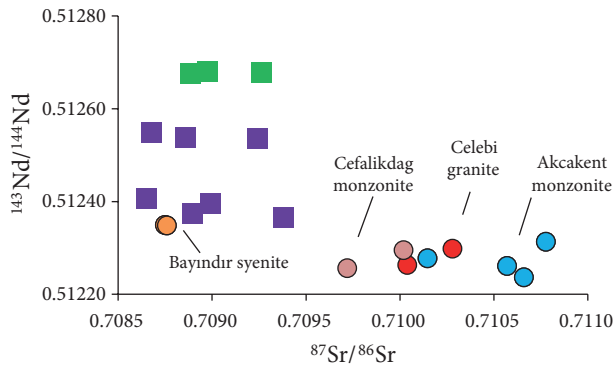
Figure 12. $^{87}Sr/^{86}Sr$ vs. $^{143}Nd/^{144}Nd$ diagram for Bayındır green and purple fluorite samples (squares). Sr-Nd isotope data on magmatic rocks (circles) are from Ilbeyli et al. (2004) and Deniz et al. (2015).

7. Conclusions

Fluorite veins in central Anatolia, except for the Pöhrenk deposit, which is hosted in limestone, were formed in alkaline magmatic rocks such as syenite and monzonite. The veins typically contain fluorite, quartz, and calcite that are accompanied by minor pyrite in Alişar and Akçakent and barite in Pöhrenk deposits. Fluorite occurs in various colors (green, purple, and yellow) and shows banding. Total rare earth + Y contents of fluorites vary in a wide range from 24 to 693 ppm. Although LREE patterns are similar, the MREE + HREE contents of green fluorites are about 10-fold higher than those of purple and yellow fluorites and host rocks as well. This implies multiple sources for the mineralizing fluids. Rare earth element ratios reveal significant fractionation and suggest that purple fluorites were crystallized at an earlier stage than green fluorites. Eu/Eu* and Ce/Ce* ratios imply that precipitation took place under low oxygen fugacities. Microthermometric measurements of fluid inclusions of fluorite yielded a broad range for homogenization temperature (86–292

°C) and salinity (0 to 20 wt.% NaCl equiv.), which are consistent values typical of a hydrothermal deposit.

In general, there is no correlation between $^{87}Sr/^{86}Sr$ ratios and fluorite color. However, $^{143}Nd/^{144}Nd$ values indicate two populations: purple fluorites are represented by less radiogenic and green fluorites are characterized by more radiogenic Nd isotope ratios. $^{143}Nd/^{144}Nd$ values of purple fluorites also form two generations with ranges significantly exceeding the analytical error. Accordingly, there are three episodes of mineralization. The Sr-Nd isotope systematics of Bayındır fluorites are conformable with those of the Bayındır syenite. This might indicate that hydrothermal fluids gradually reacted with the host rock until they were completely equilibrated.

$\delta^{18}O$ values of quartz minerals are between 10.6‰ and 15.4‰ (vs. VSMOW). $\delta^{13}C$ and $\delta^{18}O$ values of calcites are from –3.22‰ to –0.39‰ (vs. VPDB) and 9.87‰ to 13.05‰ (vs. VSMOW), respectively. Oxygen isotope compositions of quartz are not conformable with the magmatic range; rather, they suggest a contribution from meteoric and/or formation waters. Carbon isotope compositions of calcites are mostly consistent with the range of marine carbonates. Sulfur isotope values of pyrites yield a magmatic contribution. On the other hand, sulfur in barite minerals are derived either from marine or terrestrial sources. Using a temperature of 200 °C, $\delta^{18}O$ values of mineralizing fluids are estimated to be –1.6‰ to 3.2‰ (vs. VSMOW). These figures are significantly lower than those proposed for magmatic waters and possibly indicate meteoric water infiltration.

References

Aydın NS, Göncüoğlu MC, Erler A (1998). Latest Cretaceous magmatism in the Central Anatolian Crystalline Complex: review of field, petrographic and geochemical features. Turk J Earth Sci 7: 259-268.

Barker S, Bennett VC, Cox, SF, Norman MD, Gagan MK (2009). Sm–Nd, Sr, C and O isotope systematics in hydrothermal calcite–fluorite veins: implications for fluid–rock reaction and geochronology. Chem Geol 268: 58-66.

Bau M, Dulski P (1995). Comparative study of yttrium and rare-earth element behaviours in fluorine-rich hydrothermal fluids. Contrib Mineral Petr 119: 219-223.

Bodnar RJ (1993). Revised equation and table for determining the freezing point depression of H_2O-NaCl solutions. Geochim Cosmochim Ac 57: 683-684.

Bowman JR, O'Nei, JR, Essene JR (1985). Contact skarn formation at Elkhorn, Montana, II: origin and evolution of C–O–H skarn fluids. Am J Sci 285: 621-660.

Boztuğ D (1998). Post-collisional Central Anatolian alkaline plutonism, Turkey. Turk J Earth Sci 7: 145-165.

Boztuğ D, Arehart GB, Platevoet B, Harlavan Y, Bonin B (2007). High-K calc-alkaline I-type granitoids from the composite Yozgat batholith generated in a postcollisional setting following continent-oceanic island arc collision in central Anatolia, Turkey. Miner Petrol 91: 191-223.

Boztuğ D, Harlavan Y (2008). K-Ar ages of granitoids unravel the stages of Neo-Tethyan convergence in the eastern Pontides and Central Anatolia, Turkey. Int J Earth Sci 97: 585-599.

Boztuğ D, Jonckheere RC (2007). Apatite fission track data from central Anatolian granitoids (Turkey): Constraints on Neo-Tethyan closure. Tectonics 26: TC3011.

Boztuğ D, Kuşçu İ, Erçin Aİ, Avcı N (2003). Mineral deposits associated with the pre-, syn- and post-collisional granitoids of the Neo-Tethyan convergence system between the Eurasian and Anatolian plates in NE and Central Turkey. In: Eliopoulos D, editor. Mineral Exploration and Sustainable Development. Rotterdam, the Netherlands: Millpress, pp. 1141-1144.

Chesley J, Halliday A, Kyser T, Spry P (1994). Direct dating of Mississippi Valley-type mineralization; use of Sm–Nd in fluorite. Econ Geol 89: 1192-1199.

Clark ID, Fritz P (1997). Environmental Isotopes in Hydrogeology. New York, NY, USA: Lewis Publishers.

Clayton RN, O'Neil JR, Mayeda TK (1972). Oxygen isotope exchange between quartz and water. J Geophys Res 77: 3057-3067.

Deniz K (2016). Akçakent (Kırşehir) foid içerikli magmatik kayaların zamansal ve mekansal konumu. PhD, Ankara University, Ankara, Turkey (in Turkish).

Deniz K, Kadıoğlu YK (2016). Assimilation and fractional crystallization of foid-bearing alkaline rocks: Buzlukdağ intrusives, Central Anatolia, Turkey. Turk J Earth Sci 25: 341-366.

Deniz K, Kadıoğlu YK, Stuart FM, Ellam RM, Boyce A, Condon DJ (2015). U-Pb dating, whole rock and Sr-Nd-Pb-O isotope geochemistry of collisional magmatism in the CACC: Çiçekdağ igneous complex (ÇIC). Vienna, Austria: European Geosciences Union General Assembly.

Edgar AD, Arima M (1985). Fluorine and chlorine contents of phlogopites crystallized from ultrapotassic rock compositions in high pressure experiments: implication for halogen reservoirs in source regions. Am Mineral 70: 529-536.

Erler A, Bayhan H (1998). Orta Anadolu Granitoidleri ile ilişkili maden yatakları. In: Ofiyolit-granitoyit ilişkisi ile gelişen Demir Yatakları Sempozyumu, Bildiriler Kitabı, pp. 83-95 (in Turkish).

Fleischer M (1969). The lanthanide elements in fluorite. Indian Mineral 10: 36-39.

Fournier RO (1991). Water geothermometers applied to geothermal energy. In: D'amore F, editor. Application of Geochemistry in Geothermal Reservoir Development. New York, NY, USA: UNITAR, pp. 37-69.

Genç Y (2006). Genesis of the Neogene interstratal karst-type Pöhrenk fluorite–barite (± lead) deposit (Kırşehir, Central Anatolia, Turkey). Ore Geol Rev 29: 105-117.

Göncüoğlu MC, Toprak V, Kuşçu İ, Erler A, Olgun E (1991). Geology of the Western Part of the Central Anatolian Massif, Part 1: Southern Section: Unpubl. Report No. 2909. Ankara, Turkey: Turkish Petroleum Company (in Turkish).

Görür N, Tüysüz O, Şengör AMC (1998). Tectonic evolution of the central Anatolian basins. Int Geol Rev 40: 831-850.

Hein UF, Lüders V, Dulski P (1990). The fluorite vein mineralization of the southern Alps: combined application of fluid inclusions and rare earth element (REE) distribution. Mineral Mag 54: 325-333.

Hill GT, Campbell AR, Kyle PR (2000). Geochemistry of southwestern New Mexico fluorite occurrences implications for precious metals exploration in fluorite-bearing systems. Chem Geol 68: 1-20.

Hoefs J (1987). Stable Isotope Geochemistry. 3rd ed. Berlin, Germany: Springer-Verlag.

Ilbeyli N, Pearce JA, Thirwall MF, Mitchell JG (2004). Petrogenesis of collision-related plutonics in Central Anatolia, Turkey. Lithos 72: 163-182.

Kadıoğlu YK, Deniz K (2015). Orta Anadolu fluoritlerinin (OAF) Kökeni: NTE ve Sr izotop jeokimyası, Türkiye. In: Doğu Anadolu Jeoloji Sempozyumu, Bildiri Özleri Kitabı, pp. 150-151 (in Turkish).

Kadıoğlu YK, Dilek Y, Foland KA (2006). Slab break-off and syncollisional origin of the Late Cretaceous magmatism in the Central Anatolian Crystalline Complex, Turkey. In: Dilek Y, Pavlides S, editors. Postcollisional Tectonics and Magmatism in the Mediterranean Region and Asia. Boulder, CO, USA: Geological Society of America, pp. 381-415.

Koç Ş, Özşahin A, Özmen Ö (2007). A comparison between fluorite mineralizations in the Central Anatolian Massif in regard to trace element contents. Geochem Int 45: 509-517.

Köksal S, Göncüoğlu MC (2008). Sr and Nd isotopic characteristics of some S-, I- and A-type granitoids from Central Anatolia. Turk J Earth Sci 17: 111-127.

Köksal S, Göncüoğlu MC, Floyd PA (2001). Extrusive members of postcollisional A type magmatism in central Anatolia: Karahıdır Volcanics, İdiş Dağı-Avanos Area, Turkey. Int Geol Rev 43: 683-694.

Köksal S, Möller A, Göncüoğlu MC, Frei D, Gerdes A (2012). Crustal homogenization revealed by U-Pb zircon ages and Hf isotope evidence from the Late Cretaceous granitoids of the Agaçören intrusive suite (Central Anatolia/Turkey). Contrib Mineral Petr 163: 725-743.

Köksal S, Romer RL, Göncüoğlu MC, Toksoy-Köksal F (2004). Timing of post-collision H-type to A-type granitic magmatism: U–Pb titanite ages from the Alpine central Anatolian granitoids Turkey. Int J Earth Sci 93: 974-989.

Kuşçu I, Erler, A (1998). Mineralizations in the Central Anatolian Crystalline Complex: metallogeny of a collision related setting. Int Geol Rev 40: 552-565.

McDonough WF, Sun SS (1995). Composition of the earth. Chem Geol 120: 223-253.

Möller P, Dulski P, Schley F, Luck J, Szacki W (1981). A new way of interpreting trace element concentrations with respect to modes of mineral formation. J Geochem Explor 15: 271-284.

Möller P, Parekh PP, Schneider HJ (1976). The application of Tb/Ca-Tb/La abundance ratios to problems of fluorspar genesis. Miner Deposita 11: 111-116.

Munoz M, Premo WR, Courjault-Radé, P (2005). Sm–Nd dating of fluorite from the world class Montroc fluorite deposit, southern Massif Central, France. Miner Deposita 39: 970-975.

Orhan A, Mutlu H, Fallick AE (2011). Fluid infiltration effects on stable isotope systematics of the Susurluk skarn deposit, NW Turkey. J Asian Earth Sci 40: 550-568.

Özgenç İ, Şaşmaz A, Çolak M, Oyman T, İlbeyli N, Tokçaer M, Akbulut M, Karakurt, Ü (2009). Hasançelebi (Konukdere-Hekimhan-Malatya) ve Buzlukdağ (Bayındır-Kırşehir) Çevresi Alkali Kayaçlar ve Karbonatitlerle İlgili Skarn Oluşumlarının Petrolojisi, Nadir Toprak Elementleri (NTE) Jeokimyası ve Olası Cevher Odaklarının Belirlenmesi. TÜBITAK Project Final Report (Project No. 105Y076). Ankara, Turkey: TÜBİTAK (in Turkish).

Roedder E (1984). Fluid inclusions. Rev Mineral 12: 12-45.

Sánchez V, Cardellach E, Corbella M, Vindel E, Martín-Crespo T, Boyce AJ (2010). Variability in fluid sources in the fluorite deposits from Asturias (N Spain): further evidences from REE, radiogenic (Sr, Sm, Nd) and stable (S, C, O) isotope data. Ore Geol Rev 37: 87-100.

Şaşmaz A, Yavuz F (2007). REE geochemistry and fluid-inclusion studies of fluorite deposits from the Yaylagözü area (Yıldızeli-Sivas) in Central Turkey. Neues Jb Miner Abh 183: 215-226.

Şengör AMC, Yılmaz Y (1981). Tethyan evolution of Turkey-a plate tectonic approach. Tectonophysics 75: 181-241.

Seymen İ, (1981). Kaman (Kırşehir) dolayında Kırşehir Masifi'nin stratigrafisi ve metamorfizması. Türkiye Jeoloji Kurumu Bülteni 24: 101-108.

Sheppard SMF (1994). Stable isotope and fluid inclusion evidence for the origin and evolution of Hercynian mineralizing fluids. In: Seltmann R, Kampf H, editors. Metallogeny of Collisional Orogens. Prague, Czech Republic: Czech Geological Survey, pp. 49-60.

Taylor HP (1967). Oxygen isotope studies of hydrothermal mineral deposits. In: Barnes L, editor. Geochemistry of Hydrothermal Ore Deposits. New York, NY, USA: Holt, Rinehart and Winston, pp. 109-142.

Taylor HP (1978). Oxygen and hydrogen isotope studies of plutonic granitic rocks. Earth Planet Sci Lett 38: 177-210.

Taylor SR, McLennan SM (1985). The Continental Crust: Its Composition and Evolution. Oxford, UK: Blackwell.

Uras Y (2007). Pöhrenk (Kırşehir) florit yataklarının kökensel incelemesi. PhD, Çukurova University, Adana, Turkey (in Turkish).

Yalınız MK, Aydın NS, Göncüoğlu MC, Parlak O (1999). Terlemez quartz monzonite of central Anatolia (Aksaray–Sarıkaraman): age, petrogenesis and geotectonic implications for ophiolite emplacement. Geol J 34: 233-242.

Yaman S (1985). Geology and fluid inclusion studies of the fluorite deposits in the Akçakent area (Çiçekdağı-Kırşehir). Türkiye Jeoloji Kurumu Bülteni 28: 73-78 (in Turkish with English abstract).

Yılmaz S, Boztuğ, D (1998). Petrogenesis of the Çiçekdag Igneous Complex, N of Kırşehir, Central Anatolia. Turk J Earth Sci 7: 185-199.